South African Journal of Chemical Engineering 44 (2023) 14–30

Contents lists available at ScienceDirect

South African Journal of Chemical Engineering

journal homepage: www.elsevier.com/locate/sajce

Recent trend of metal promoter role for CO_2 hydrogenation to C_1 and C_{2+} products

Novia Amalia Sholeha [a,b], Holilah Holilah [b,c], Hasliza Bahruji [d,*], Athirah Ayub [d], Nurul Widiastuti [c], Ratna Ediati [c], Aishah Abdul Jalil [e,f], Maria Ulfa [g], Nanang Masruchin [b,h], Reva Edra Nugraha [i], Didik Prasetyoko [c,*]

[a] College of Vocational Studies, Bogor Agricultural University (IPB University), Jalan Kumbang No. 14, Bogor 16151, Indonesia
[b] Research Center for Biomass and Bioproducts, National Research and Innovation Agency of Indonesia (BRIN), Cibinong 16911, Indonesia
[c] Department Chemistry, Faculty of Science and Data Analytics, Institut Teknologi Sepuluh Nopember, Kampus ITS Keputih, Sukolilo, Surabaya, 60111, Indonesia
[d] Centre of Advanced Material and Energy Science, Universiti Brunei Darussalam, Jalan Tungku Link, BE 1410, Brunei
[e] Department of Chemical Engineering, Faculty of Chemical and Energy Engineering, Universiti Teknologi Malaysia, 81310 UTM, Skudai, Johor Bahru, Johor, Malaysia
[f] Centre of Hydrogen Energy, Institute of Future Energy, Universiti Teknologi Malaysia, Skudai, 81310 UTM, Skudai, Johor Bahru, Johor, Malaysia
[g] Chemistry Education Study Program, Faculty of Teacher Training and Education, Sebelas Maret University, Jl. Ir. Sutami 36A, Surakarta 57126, Indonesia
[h] Research Collaboration Center for Biomass and Biorefinery between BRIN and Universitas Padjadjaran, Jatinangor 45363, Indonesia
[i] Department of Chemical Engineering, Faculty of Engineering, Universitas Pembangunan Nasional "Veteran" Jawa Timur, Surabaya, East Java, 60294, Indonesia

ARTICLE INFO

Keywords:
CO_2
Hydrogenation
Metal promoter
C_1 products
C_{2+} products

ABSTRACT

CO_2 hydrogenation as sustainable route for generation of value-added carbon feedstock is identified as green pathway for mitigation of greenhouse gasses emission. CO_2 methanation is one of the promising solutions, which only requires reactions at atmospheric pressure while utilizing metal catalysts to overcome kinetic limitations. Metal catalysts can be promoted to alter reducibities, CO_2 adsorption capacities, and H_2–CO_2 dissociation potential. The role of metal promoter such as rare earth elements (Ce, Mn, Co, and La) and alkali and alkali earth metal (Li, Na, Ca, and K) will be discussed within the scope of CO_2 methanation. The aspect of catalysts modification towards hydrogen dissociation potential and surface oxygen vacancy will be emphasized to enhance selectivity for methane. Another pathway for CO_2 hydrogenation is via further conversion into longer chain molecules such as olefin and ethanol. The benefit of metal promoter will be discussed in this review on the effect towards promoting C—C coupling reaction for producing longer chain alcohol and light olefin. The strategies to develop active catalysts for the coupling reaction of C—C will be emphasized with the promoter introduction. For the hydrogenation of CO_2 to longer chain molecules, the main metal catalysts Ni, Pd, Rh, and Co, and their modification with promoter such as Ga, Cu, and alkali metal Na, K will be discussed. A critical analysis of the CO_2 methanation mechanism and further C—C reaction to longer chain molecules will be discussed, particularly the effect of metal promoters to stabilize the intermediate and maneuver the catalytic reaction pathway into the desired products.

1. Introduction

Reliance on fossil fuels as a primary energy source inevitably leads to the accumulation of carbon dioxide in the atmosphere. The rising level of atmospheric CO_2 has led to global warming and devastating climate deterioration. Based on IEA data published in Global Energy and CO_2 Status Report, CO_2 emissions are determined at 32.5 gigaton (Gt) in 2017, a significant 1.4% increase from 2016. The value is 55% higher than the past 25 years and is predicted to further increase by 10% in 2040. Moreover, the global average temperature rise exceeds 1.5 °Celsius (°C) around 2030 and continues to rise until it reaches 2.6 °Celsius (°C) in 2100 (I.E. Agency 2022). CO_2 technology is mainly circumventing two main approaches: carbon capture and storage (CCS) or carbon capture and utilization (CCU) as illustrated in Fig. 1. CO_2 capture, either via oxy-combustion, pre-combustion, or post-combustion captures, can be adapted depending on the sources of CO_2 emission (Atsbha et al., 2021). The most fundamental concept of CCS is capturing and compressing CO2 gasses to prevent emissions into the atmosphere

* Corresponding authors.
E-mail addresses: hasliza.bahruji@ubd.edu.bn (H. Bahruji), didikp@chem.its.ac.id (D. Prasetyoko).

https://doi.org/10.1016/j.sajce.2023.01.002
Received 30 August 2022; Received in revised form 21 December 2022; Accepted 4 January 2023
Available online 11 January 2023

(Fu et al., 2022). Another CCS technique involves the sequestration of CO2 in geologically stable sites; however, the operational cost is considered high, and the viability of CO2 as a carbon source is not fully utilized.

CCU technology, subsequent capture and utilization of CO_2, is more beneficial than CCS since the value-added goods derived from CO_2 usage could be applied as a revenue source during the mitigation of CO_2. Furthermore, unlike CCS, there is no possibility of CO_2 leakage with CCU, making this technology environmentally friendly and sustainable. Fig. 2a summarised the number of reported publications on CO_2 conversion into value added chemicals from 2010 to 2021. Carbon dioxide utilization was mostly reported via photocatalytic reactions, electrochemical reduction, and thermochemical-catalytic hydrogenation. The electrocatalytic reduction of CO_2 depends on the pH and the electrode voltage, and is conducted at ambient temperature and pressure (Ruiz-Lopez et al., 2022). Activating the extremely stable CO_2 molecule needs a significant overpotential; consequently, the CO_2 reduction is hampered by the side hydrogen evolution reaction (HER) (Yu et al., 2023). Photocatalytic CO_2 hydrogenation utilized photoexcitation energy carriers on semiconductor photocatalysts, to undergo a series of reduction and oxidation reaction (Zhang et al., 2021). In contrast to typical thermal catalysis, the photocatalytic conversion of CO_2 exhibited lower performance and the photocatalysts often has inefficient light absorption and faster recombination (Fan and Tahir, 2022). Another pathway of CO_2 utilization is via mineralization and biofixation, direct used as a solvent, particularly in a CO_2 supercritical environment, and used in food and beverage industries.

1.1. Thermocatalytic conversion of CO_2

The thermochemical process is favorable for CO_2 conversion since the process has high energy and conversion efficiency. In the presence of thermal heat energy, CO_2 was converted into various products such as methanol, methane, dimethyl ether, syngas ($CO + H_2$), and higher alcohol and hydrocarbons, which depend on the catalysts, pressure, and temperature. Thermocatalytic CO_2 valorization employed either heterogeneous or homogeneous catalysts and can be conducted in gas and liquid phase conditions (Ojelade and Zaman, 2021). CO_2 methanation promises a high conversion of CO_2 at atmospheric pressure. Methane production from CO_2 can be integrated into the power grid via a Power to Gas (PtG) plant, which has a higher potential for providing baseload electric power than wind or solar energy due to their intermittent nature (Schaaf et al., 2014). CO_2 conversion to alcohol and olefins is appealing for industrial processes as the products obtained have a higher demand. Apart from that, the production of liquefying hydrocarbons is advantageous for easy storage and transportation. For the hydrogenation to long chain molecules, the catalyst promotes the coupling of C—C reaction of CO* or CH_3* intermediets. The reaction is often conducted at high temperatures, i.e., 400 °C, and at high pressures of up to 20–50 bar (Ye et al., 2019). Over the years, various catalysts, such as hydrotalcite-derived catalysts (Liu et al., 2022), cobalt metal organic frameworks (MOFs) (Keen and Tahir, 2022), Cu-based catalysts (Niu et al., 2022), tandem methanol synthesis (Xiao-xing et al., 2022), nanoparticle catalysts (Sharma et al., 2022), and N-doped carbon-based materials (Adegoke and Maxakato, 2022) were investigated for CO_2 hydrogenation. Different types of transition metals catalyst (Ni, Ce, Co, Cu, Fe), with noble metal promoters (Pd, Au, Rh), and alkali metals (Na, Li, K) changed the selectivity of CO_2 methanation to longer chain molecules, such as ethanol and ethylene Fan et al. (Fan and Tahir, 2021) reported the synergy between supports and active metals in promoting CH_4 generation, which can be optimized for the advancements of hydrogenation reaction. Metal promoter introduces additional active sites for optimizing the distribution of products to yield the desired hydrocarbons. Fig. 3 correlates the results from reported studies on Fe/Al_2O_3 catalysts with different types of metal promoters toward the formation of C_1, C_2—C_4, and C_{5+} products formation. Metal promoters such as Ni enhanced the activity of Fe/Al_2O_3 towards CH_4 formation (Valinejad Moghaddam et al., 2018; Burger et al., 2018), whereas Cu prolonged the stability of intermediates to generate C_2—C_4 products (Chaipraditgul et al., 2021; W. Wang et al., 2018). Co on Fe/Al_2O_3 catalysts showed selectivity towards CH_4, C_2—C_4 hydrocarbons, and C_{5+} products, with the selectivity being closely associated with the amount of Co loading (Satthawong et al., 2013). Several comprehensive reviews on CO_2 hydrogenation listed in Table 1 have focused on the recent trends in catalyst design for CO_2 hydrogenation. The role of promoters in changing the course of CO_2 hydrogenation has gained considerable

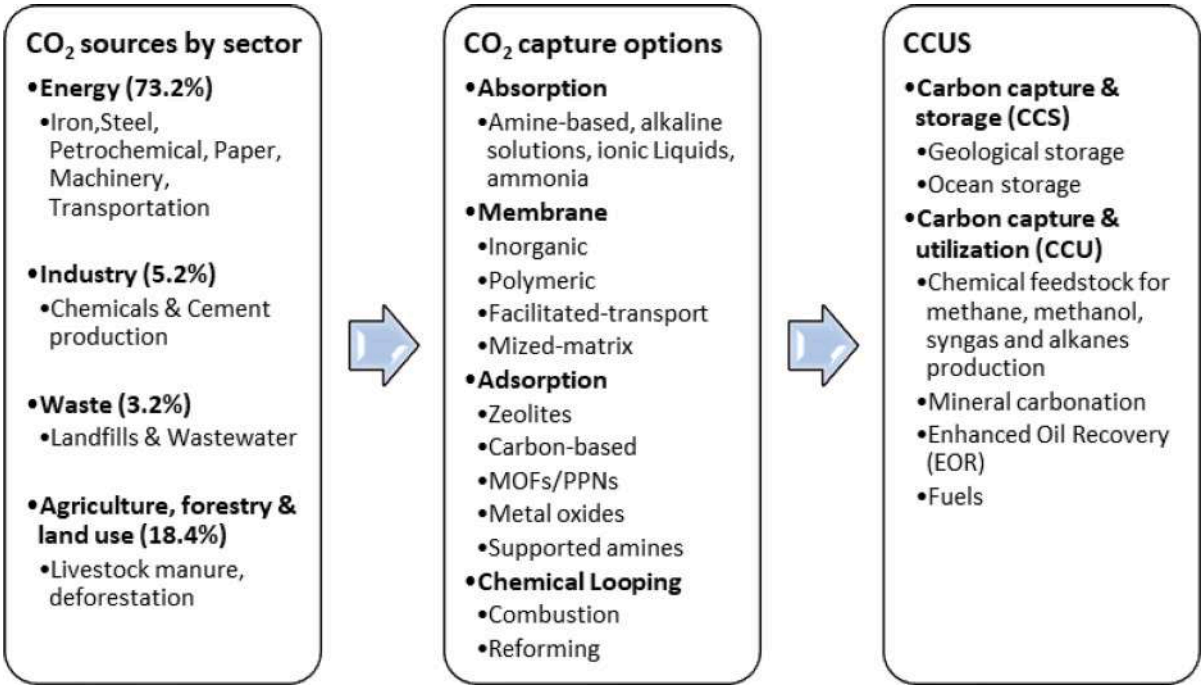

Fig. 1. Current technology of carbon capture, utilization, and storage (CCUS) (Ritchie et al., 2020; Al-mamoori et al., 2017; Cuellar-Franca and Azapagic, 2015).

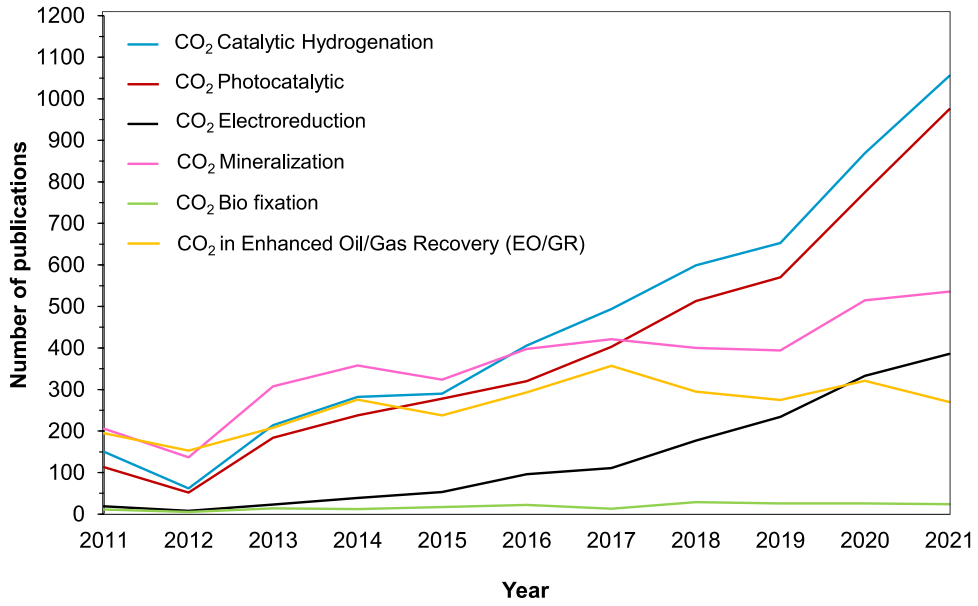

Fig. 2. Number of publications on CO_2 Capture and Utilization (CCU) since 2011–2021 (Source: www.scopus.com).

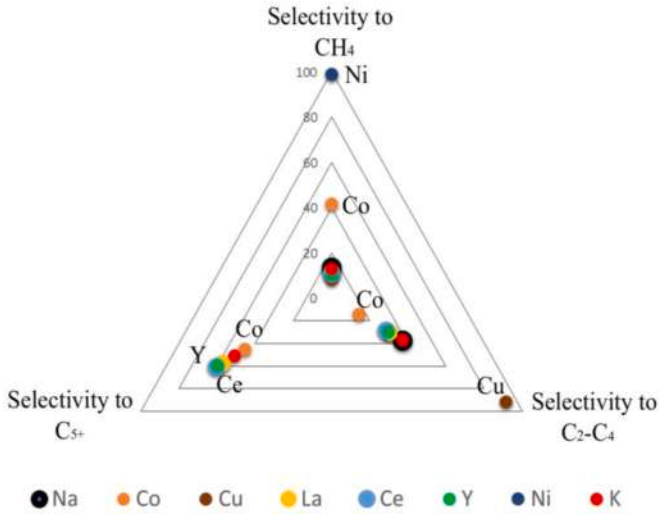

Fig. 3. Correlation between products selectivities and metal promoters on the activity of Fe/Al_2O_3 catalysts.

Table 1
The recent reviews of CO_2 utilization.

No.	Focus	Ref.
1	Factor in photocatalysts TiO_2 for CO_2 conversion to hydrocarbon fuels: particle size and shape, temperature, surface area, modification techniques, and surface sensitization	(Hossen et al., 2022)
2	The catalysts of cobalt heterosite in higher alcohols production from carbon dioxide	(Liu et al., 2023)
3	MOF-based catalysts in the CO_2 hydrogenation to synthesize products such as CO, CH_4, methanol, formic acid, and C_{2+} products	(Shao et al., 2022)
4	Cu-based bimetallic catalysts reduction reaction of CO_2	(Wang et al., 2022)
5	Nanobiomaterials and nanocatalyst for CO_2 converting to CH_4	(Sharma et al., 2022; Raza et al., 2023)
6	The metal promoter effects on CO_2 hydrogenation	This review

interest in the conversion of CO_2 into various hydrocarbon products. Therefore, this review provides a comparative discussion of current findings to understand the effect of promoters on product selectivity and the mechanistic steps of CO_2 hydrogenation and C—C coupling reactions. Understanding the fundamentals of CO_2 hydrogenation allows the interception of intermediates to undergo the C—C coupling reactions for the generation of long carbon chain molecules. After establishing the fundamentals and mechanism of reaction, the review will further discuss transforming CO_2 methanation catalysts into active catalysts for the synthesis of higher hydrocarbon/alcohol by incorporating various promoters.

2. Reaction mechanism

2.1. CO_2 hydrogenation to C_1 products

2.1.1. CO_2 methanation

CO_2 conversion into CH_4 as a C_1 product is observed not only as a CO_2 remediation route but also as hydrogen storage. The CO_2 conversion to methane is advantageous in the thermodynamic aspect compared to the conversion of CO2 into methanol or a higher hydrocarbon.

$$CO_2 + 4\,H_2 \rightarrow CH_4 + 2\,H_2O \left(\Delta H^{\circ}_{298} = -165 \frac{kJ}{mol}\right) \quad (1)$$

$$CO_2 + 4\,H_2 \rightarrow CH_3OH + 2\,H_2O \left(\Delta H^{\circ}_{298} = -49.5 \frac{kJ}{mol}\right) \quad (2)$$

CO_2 methanation is an exothermic process operating at temperatures between 150 °C and 550 °C. CO_2 methanation can proceed through direct methanation, also widely recognized as Sabatier reaction that involves formate as an intermediate. The second pathway requires the dissociation of two CO molecules to form C and CO_2 gas. This reversible exothermic reaction is known as the Boudouard reaction. But in general, CO_2 methanation begins with the dissociation of carbon dioxide to carbon monoxide via the water gas shift (WGS) reaction (Eq (3)). This followed by the subsequent CO hydrogenation to methane (Eq (4)) (Schaaf et al., 2014). The Sabatier reaction is dominant at low temperatures, and the reverse water gas shift (RWGS) reaction is only favored at higher reaction temperatures (an endothermic reaction) (Mutschler et al., 2018). Thus, CO_2 methanation is optimally carried out at temperatures below 500 °C. High concentrations of CO_2 also contributed to

the deactivation of catalyst due to the formation of hot spots, metal sintering, and coke deposition, resulting in a decrease in product yield. For these reasons, the catalyst should have thermal stability at low and high temperatures (Janke et al., 2014).

$$CO_2 + H_2 \leftrightarrow CO + H_2O \left(\Delta H^{\circ}_{298} = 41 \frac{kJ}{mol}\right) \quad (3)$$

$$CO + 3\,H_2 \leftrightarrow CH_4 + H_2O \left(\Delta H^{\circ}_{298} = -206.3 \frac{kJ}{mol}\right) \quad (4)$$

Fig. 4 depicts the schematic mechanism of CO_2 methanation. CO_2 was adsorbed generally on the support via physisorption and chemisorption (Step 1). The amount of adsorbed CO_2 depends on the physicochemical properties of support, such as surface area, basicity, and surface oxygen vacancies. The CO_2 dissociation route in CO_2 methanation produces CO and C, depending on the density of surface oxygen vacancy on the support (Step 2). Supports with abundant surface oxygen vacancies such as zeolite (Bacariza et al., 2019; Sholeha et al., 2020; Sholeha et al., 2021; Bahruji et al., 2022), mixed oxide (Mebrahtu et al., 2018; Panagiotopoulou, 2017; Li et al., 2018), mesostructured silica (Aziz et al., 2014) and hydrotalcite (HT) (Liu et al., 2022) were commonly utilized to initiate CO_2 dissociation. CO dissociation requires more activation energy (Ea = 286.56 kJ mol^{-1}) than CO_2 dissociation (Ea = 122.54 kJ mol^{-1}). CO formation was also reported to follow the formation of formate intermediates (Sakpal and Lefferts, 2018). CO_2 occupies the oxygen vacancy and is hydrogenated into formate intermediates. Metal catalyst is crucial for hydrogen dissociation to reduce adsorbed CO_2 (Step 3). *In-situ* FTIR spectroscopy studies indicated that the adsorption and dissociation of CO_2 and H_2 occur on metal sites to form CO, O, and H. The dissociated CO interacted with oxide surfaces from the support materials to form bridged and linear carbonyl. The presence of H atoms facilitated the formation of bidentate formate (Teh et al., 2015).

The Boudouard reaction requires the dissociation of two CO molecules to form C and CO_2 gas. At elevated temperatures, the reverse Boudouard reaction becomes favorable as the Gibbs free energy of the formation decreases. A study by Cheng et al. (Teh et al., 2015) reported that C—O bond dissociation is not favorable on well-aligned transition metals due to weak interactions. The activation energy calculated from these two reaction steps indicates that the second pathway is favorable. CH_4 formation from derivative carbon generally requires much less activation energy. The dissociated carbon species underwent subsequent hydrogenation steps to produce CH_4.

$$CO_2 \rightarrow CO + O \left(Ea = 122.54 \frac{kJ}{mol}\right) \quad (5)$$

$$CO_{(ads)} \rightarrow C_{(ads)} + O_{(ads)} \left(Ea = 286.56 \frac{kJ}{mol}\right) \quad (6)$$

$$2\,CO_{(ads)} \rightarrow C_{(ads)} + CO_{2(ads)} \left(Ea = 186.22 \frac{kJ}{mol}\right) \quad (7)$$

$$C + H \rightarrow CH \left(Ea = 69.47 \frac{kJ}{mol}\right) \quad (8)$$

$$CH + H \rightarrow CH_2 \left(Ea = 50.17 \frac{kJ}{mol}\right) \quad (9)$$

$$CH_2 + H_2 \rightarrow CH_4 \left(Ea = 48.20 \frac{kJ}{mol}\right) \quad (10)$$

The mechanism of CO_2 methanation is still continuously investigated, particularly on identifying the nature of reaction stages and the intermediate species. Nevertheless, the mechanism can be divided into two pathways, CO route and formate intermediates. On the CO pathway, CO_2 is converted to adsorbed carbonyl (CO_{ad}), subsequently reacted with H_2 to form CH_4. Direct CO_2 dissociation into O_{ad} and CO_{ad} or via the formate ($HCOO_{ad}$) species decomposition have been ascribed as the origin of CO_{ad}. Formate became the primary intermediate when no CO_{ad} was detected during the reaction. The evolution of surface species was monitored using DRIFTS (diffuse reflectance infrared Fourier transform spectroscopy). CO and formate intermediate routes can be clearly distinguished using Ni/ZrO_2—C produced from conventional impregnation, and Ni/ZrO_2-P synthesized from plasma-assisted impregnation (Jia et al., 2019). Ni/ZrO_2-P is postulated to follow CO pathway, in which CO_2 is transformed to monodentate and bidentate bicarbonates via reactions between adsorbed CO_2 and hydroxyl (OH) group. The monodentate and bidentate bicarbonates reacted with hydrogen atoms to produce monodentate and bidentate formates. Formate decomposed into CO_{ads}, and subsequently hydrogenated to CH_4. The absence of carbonyl species during DRIFTS analysis implies the mechanism of the formate pathway on Ni/ZrO_2—C. CO_2 gas reacted with OH groups formed the main intermediate species, such as bidentate formates and bidentate bicarbonates. Formates are converted into methoxy before the subsequent hydrogenation of methoxy (OCH_3) to CH_4.

Another study suggested that the carbonyl species formed through CO_2 dissociation (Aziz et al., 2014). On the meso-structured silica (MSN), the adsorbed CO_2 and H_2 at active metal sites dissociated into CO, O, and H atoms. Carbonyl species are produced by the reaction of carbon monoxide with oxide surfaces, together with the generation of bidentate formate following the reaction with H atoms. Concurrently, the reaction between the adsorbed dissociated oxygen and the H atom produces hydroxyl, which reacts with a second H atom to make H_2O. The carbonyl bridge and bidentate formate are hydrogenated further to generate CH_4.

Yang et al. (2020) undertook theoretical studies by density functional theory to determine the intrinsic CO_2 methanation reaction and active site over Rh/TiO_2 catalyst. The metal-support interfaces accumulated charges that provide electrons for the reduction of CO_2 to

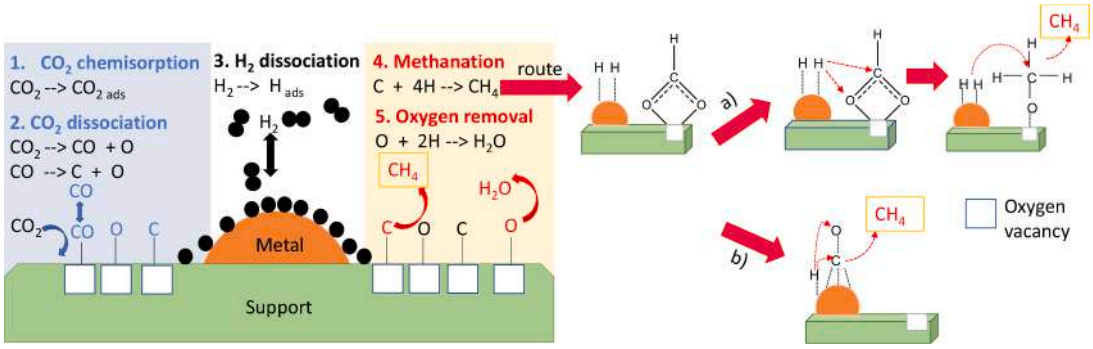

Fig. 4. Schematic mechanism of CO_2 methanation via a) dissociation route and b) formate decomposition route.

produce CH_4. CO_2 adsorption and activation were more feasible at the metal-support interface than at the Rh nanoparticle's perimeter. The RWGS + CO hydrogenation via the COH* intermediate is the thermodynamically and kinetically preferred approach over Rh/TiO_2 catalyst compared to the direct C–O bond breakage pathway and the formate pathway. Higher activation energy barriers inhibit the direct C–O bond cleavage and formate pathways. The combination of the molecular orbital polarization and H—O bond formation (COH*) is intimately related to the CO* activation generated by the RWGS reaction. CO_2 hydrogenation to CH_4 over Rh/TiO_2 catalyst happens mainly through the primary pathway i.e., CO_2* → COOH* → CO* → COH* → HCOH* → H_2COH* → CH_3* → CH_4* (Fig. 5).

2.1.2. CO_2 to methanol

CO_2 hydrogenation to methanol is a primary reaction for Gas to Liquid (GTL) conversion of CO_2 (Nezam et al., 2021). Methanol is a raw material to produce fuels in methanol-to-olefins (MTO) and methanol-to-gasoline (MTG). Methanol is also the precursor for BTX aromatics, formaldehyde, acetic acid, methyl methacrylate, dimethyl terephthalate, methylamines, chloromethane, dimethyl carbonate and methyl tertbutyl ether (MTBE) (Arandia et al., 2023). Methanol is also identified as an alternative fuel replacement as it burns cleanly, is highly biodegradable, can combine with gasoline, and can reform into hydrogen. Iceland has become the primary industrial reference for sustainable methanol synthesis from CO_2 and H_2 using geothermal energy (Tountas et al., 2019). The country has an annual methanol capacity of 4000 t and valorizes 5600 tons of CO_2.

The exothermic methanol production from CO_2 hydrogenation requires low temperatures and high pressures (Eq. (11) and Eq. (12)). However, temperatures exceeding 200 °C are required to reach a satisfactory conversion due to CO_2 low reactivity. Under high temperatures, CO_2 hydrogenation to methanol is in competition with rWGS (Eq. (3)). The rWGS produces a substantial amount of H_2O, which inhibits the equilibrium conversion of CO_2. Water is detrimental to the stability of

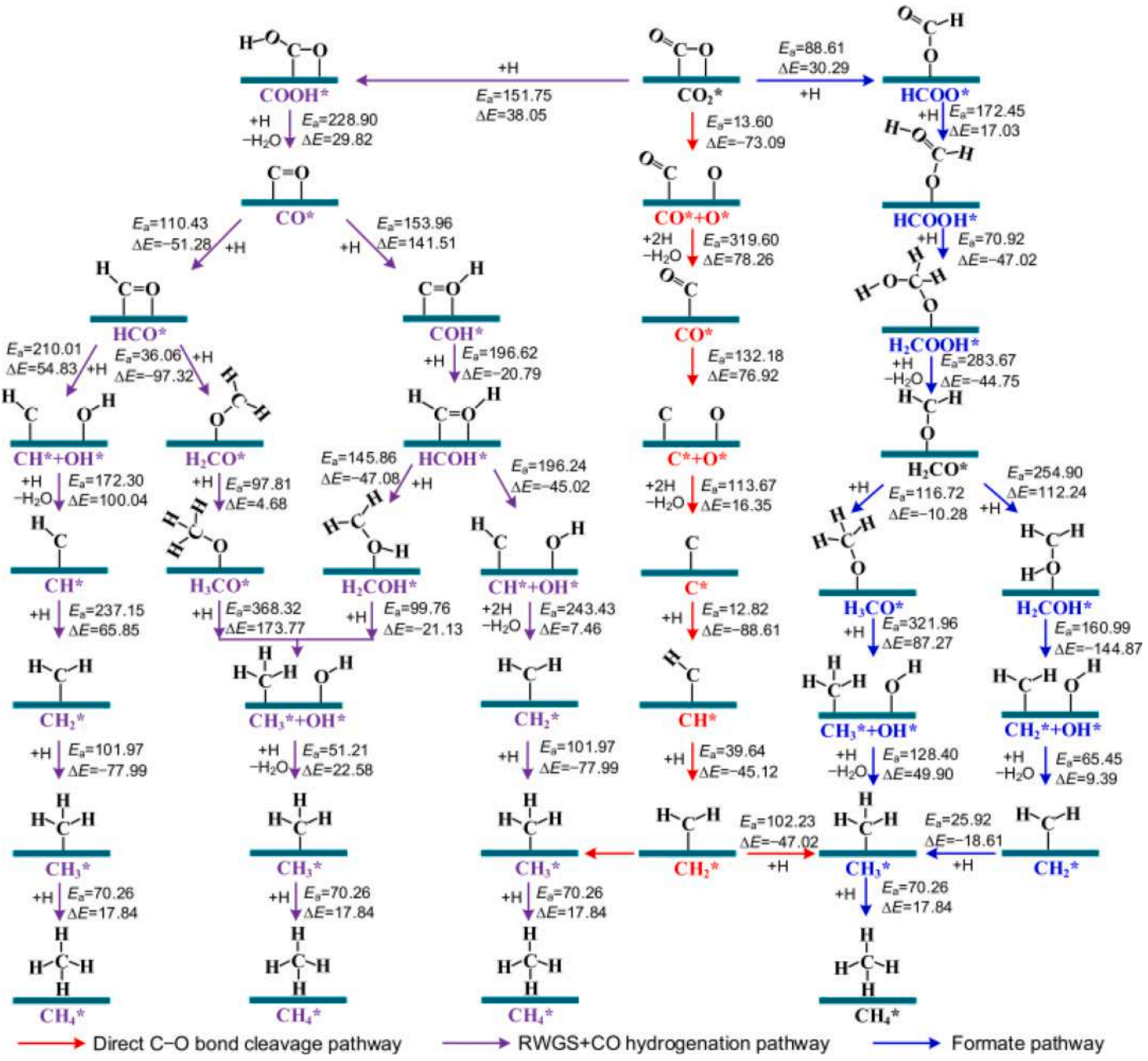

Fig. 5. Proposed CO_2 methanation pathways over Rh/TiO_2 catalyst from ref. (Yang et al., 2020). Copyright © 2020 Elsevier.

catalysts and promotes deactivation.

$$CO + 2\,H_2 \leftrightarrow CH_3OH \quad (11)$$

$$CO_2 + 3\,H_2 \leftrightarrow CH_3OH + H_2O \quad (12)$$

$$2\,CH_3OH \rightarrow CH_3OCH_3 + H_2O \quad (13)$$

$$n\,CH_3OH + H_2 \rightarrow CH_3(CH_2)_{n-2}CH_3 + H_2O \quad (14)$$

$$n\,CH_3OH \rightarrow CH_2 = CH(CH_2)_{n-3}CH_3 + n\,H_2O \quad (15)$$

CO_2 hydrogenation to methanol requires active sites for stabilizing the formate and methoxy intermediates. The mechanism follows similar preliminary steps as methanation. CO_2 adsorbed as linear or bridging carbonates, that subsequently hydrogenated to formate species. DRIFTS analysis on PdZn/TiO_2 indicates the broad adsorption band of C—O stretch in methoxy, *OCH_3 appeared in PdZn/TiO_2 at 200 °C, 15 bar. The transformation from formate and CO intermediates into methoxy species requires high pressures. The methoxy bands were accompanied by C—H stretching that only occurs on PdZn alloy but is absent on Pd metal. PdZn/TiO_2 eliminates methane formation, by stabilizing the methoxy species, for further hydrogenation to methanol (Bahruji et al., 2022). On a hybrid PdZn/TiO_2 with ZSM-5, the C—O band from the adsorbed methoxy *OCH_3 appeared less intense. However, two adsorption bands corresponded to C—O-C stretch of adsorbed DME and *OCH_3 of adsorbed DME occurred at 100 °C. The desorbed methanol molecules from the active metal catalyst re-adsorbed on the solid acid zeolite to generate methoxy groups for DME formation (Ye et al., 2019). Ye et al. (Attada et al., 2022), stated that CO_2 hydrogenation based on a methanol (CH_3OH) reaction can be achieved by combining two sequential processes over a bifunctional catalyst. First, CO_2 and H_2 are transformed to CH_3OH via a CO or formate pathway over a partly reduced oxide surface (e.g., Cu, In, and Zn) or noble metals. Bifunctional or hybrid catalysts consist of a CH_3OH synthesis catalyst and a CH_3OH dehydration/coupling catalyst, converting CO_2 into high-value C_{2+} molecules such as DME, gasoline-like hydrocarbons, and light olefins. Under the same conditions, an effective catalyst for these high-value C_{2+} products should be active for CH_3OH synthesis and dehydration/coupling (Fig. 6).

2.1.3. CO_2 to CO

CO is more reactive than CO_2 and a crucial intermediate in the manufacture of methane, methanol, DME, and hydrocarbons, which explains why synthesis gas (CO and H_2) is employed as feedstock in industry (Eq. (16)). The conversion of CO_2 to CO is often conducted via dry reforming of methane and reverse water gas shift reaction. The reaction is endothermic, which necessitates temperatures above 700 °C for significant CO_2 conversion. Redox and dissociative mechanisms are the most frequently reported for rWGS reaction. H_2 is not a reactant in the redox mechanism, although it does diminish the surface of the catalyst. The active sites for CO_2 dissociation are metallic crystals, and the oxidized metallic sites are reduced, releasing H_2O, and regenerating the metallic sites (Eq. (16) and Eq. (17)). H_2 combines with CO_2 in the dissociative mechanism, resulting in the creation of formate species (HCO_2_M), which immediately releases CO. These formate species are created by the attack of OH groups on M-CO species and MO_2H species, formed via intermediate CO_2-metal protonation. According to this process, it has been confirmed that the presence of surface hydroxyl groups facilitates CO_2 adsorption and hydrogenation (Ateka et al., 2022).

$$CO_2 + M^0 \rightarrow Cu_2O + CO \quad (16)$$

$$H_2 + MO \rightarrow H_2O + M^0 \quad (17)$$

Most of the studies investigated synthesis gas formation (CO + H_2) from CO_2 via dry reforming with methane to exclude the use of hydrogen as reducing agent. CO_2 reacts with methane at high temperatures releasing equal molars of CO and H_2 gasses (Eq. (18)).

$$CO_2 + CH_4 \leftrightarrow 2\,CO + 2\,H_2 \left(\Delta H^{\circ} = 261 \frac{kJ}{mol}\right) \quad (18)$$

CO formed from CO_2 is via associative mechanism on support such as MgO, TiO_2 or Al_2O_3, with the formation of carbonate and formats is considered as the rate limiting steps. Dry reforming via in-situ IR conducted on $MgAl_2O_4$ indicates the formation of monodentate carbonate species formed on strongly basic surface O^{2-} ions (Azancot et al., 2021). The carbonate adsorbed mainly as linear or bridged carbonate, although bridged carbonate was reported at much lower concentrations, particularly on a strong basic support (Azancot et al., 2021). The carbonyl hydrogenated into bicarbonates via reaction with surface hydroxyl group. The bicarbonate further reacted with H_2 gas to form formate (HCOO-) and water. In dry reforming of methane, the addition of CH_4 is crucial for the formation of formate species. H_2 was dissociated form CH_4 on metallic surfaces such as Ni, Ru and Pt via consecutive H abstraction. However, in the absence of hydrogen, formate can be produced via reaction with physisorbed water on the catalysts or surface hydroxyl group. The bands ascribed to the asymmetric C–O stretching and to the H–C–O bending modes of formate in infrared spectra appeared with unchanged intensity over time (Ferreira-Aparicio et al., 2000). On Pt/ZrO_2, Rh/TiO_2 catalysts (Nakamura et al., 1994), the formate-like intermediate occurred on the support or metal-support interface.

The dissociated CHx and H_{ad}. subsequently reacted with the

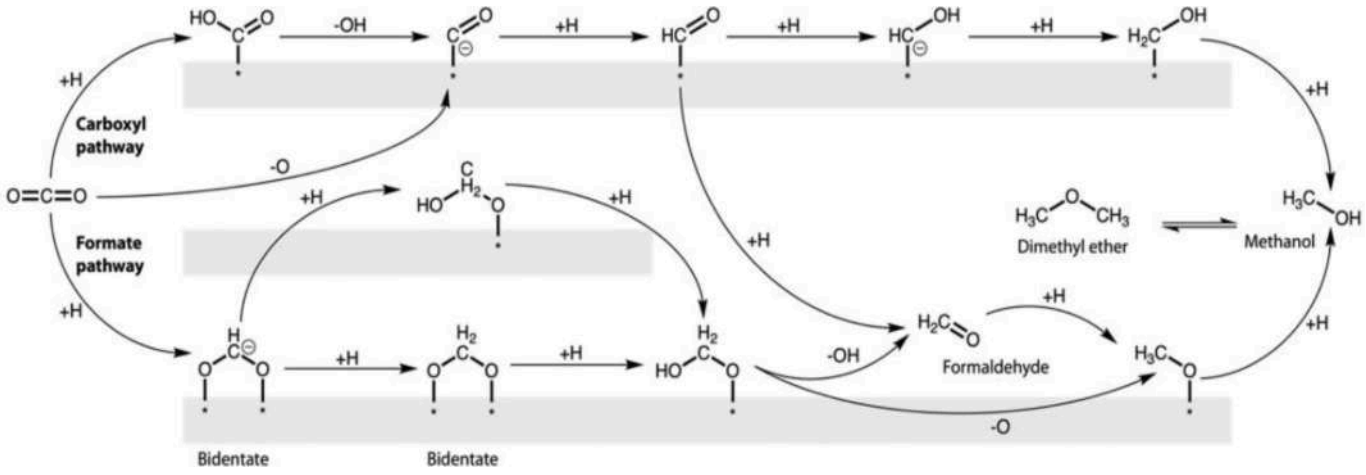

Fig. 6. Possible reaction in methanol production from ref (Attada et al., 2022). Copyright © 2022 Elsevier.

adsorbed CO_2 to accelerate CO_2 dissociation to form another CO molecule and H_{ads}. As the CO leaves the surface, H adsorbed predominantly on metallic sites such as Ni, Ru and Pt desorbed as H_2 gas. CH_4 activation often occurred on metallic sites, via dissociative mechanism to form CH_x and H_{ads}. CH4 dissociation is also reported on SBA-15 via interaction of H-atom with the oxygen atom in silanol group. Unidentate carbonates, bidentate carbonates and linear carbonyls were identified as the intermediate species in dry reforming, that subsequently reacted with CH_4 to form CO and H_2 gasses. CO_2 was suggested to occupy the oxygen vacancy on SBA-15 support, while CH_4 adsorbed on Ni metallic surfaces to form CH_x and H species (Chong et al., 2020).

2.2. CO_2 hydrogenation to C_{2+} products

Most reported studies on the CO_2 hydrogenation mechanism to C_{2+} (higher hydrocarbons/alcohol) were conducted via in-situ DRFITS analysis. Occasionally, NMR was also employed, as summarized in Table 2. Fig. 7 illustrates the suggested mechanism of the C—C coupling reaction in CO_2 hydrogenation. Generally, the reaction was initiated via the same steps reported in CO_2 methanation. CO_2 adsorption on the catalyst surface occurred via carboxylate or bidentate carbonate formation, while hydrogen adsorption and dissociation occurred on metal surfaces. The presence of surface hydroxyl or oxygen vacancies on the support weakens and dissociates the first C—O bond in CO to form CO. CO_2 has also been reported to adsorb and activate to form formate intermediates, which are then converted to *CO and *CH_3 (Bai et al., 2017). The crucial aspect of the C—C coupling reaction involves the stabilization of *CO and *CH_3 intermediates. The insertion of CO molecules that were produced from the RWGS reaction into CH_x intermediates initiated the first coupling reaction during the hydrogenation of CO_2. Studies reported by Zhang et al. (S. Zhang et al., 2020) observed simultaneous adsorption of CO and CH_x bands, suggesting that the CO formed from RWGS was hydrogenated to form CH_x. Later, the CO and CH_x reacted, triggering the C—C coupling reaction (S. Zhang et al., 2020).

Controlling the hydrogen dissociation activity of metal catalysts to enhance the C—C coupling reaction was reported for Rh based catalysts. CO was adsorbed linearly or formed a bridge on the Rh surface, which occupied most of the Rh available active sites. As a result of strongly held CO molecules forming on the Rh surface, H_2 dissociation is prevented, and thus methane formation is suppressed (Kusama et al., 1996). CO also reacted with CH_3O* species to form ethanol, as observed on Ir-In_2O_3 single atom catalysts. At 200 °C, DRIFTS analysis revealed a high concentration of adsorbed CO species in the presence of methoxide, CH_3O*. The results were further supported by $^{13}CH_3OH$ isotope experiment that showed the stable intermediates were CO* and CH_3O*, crucially important for C—C coupling to produce ethanol (Ye et al., 2020).

The rate determining step of the C—C coupling reaction to form ethanol is suggested to involve the hydrogenation of adsorbed *CO to formyl (*HCO) species (Yang et al., 2019). The presence of a high density hydroxyl group, as reported on RhFeLi/TiO_2 catalysts, enhanced the formation of formyl HCO* species. The adsorbed formyl (HCO*) was also more likely to dissociate into CH_x than CO, thereby initiating the C—C coupling reaction, as evidenced by the significant amount of CH_3* species detected by DRIFTS analysis (Yang et al., 2019). The hydroxyl group was also suggested to enhance C—O bond scission in formyl species to form CH_x intermediates for the C—C coupling reaction. Further investigation with 1H MAS NMR analysis indicated that the signal assigned to *CH_3 and *CH_2 species bonded to the oxygen on the catalyst's surface was more favorable than further hydrogenation. *CH_3 prefers to couple with *C1-oxygen to form C_2-oxygen species rather than undergo deep hydrogenation to form methane, which might explain the undetectable methane (L. Wang et al., 2018). Apart from that, CH_x* insertion into *HCOO was also proposed as another plausible mechanism for the C—C coupling reaction to form ethanol. In-situ FTIR of CO_2 hydrogenation on $NiCOAl_2O_3$ catalysts revealed the formation of abundant *HCOO species earlier in the reaction than *CH_x. The signal weakens, followed by the continous formation of *CH_3COO and *C_2H_5O intermediates (Wang et al., 2019).

Table 2
A summary of the intermediate species observed in CO_2 methanation, and C—C reactions obtained from FTIR and NMR analysis.

Intermediate species	FTIR band (cm^{-1})	1H NMR (ppm)	13C NMR (ppm)
*CO Linear Bridge	2040 and 1860 (Kusama et al., 1996)	–	–
CO_3^{2-} (carbonate)	1400, 1490 and 1645 (Solymosi et al., 1981)	–	170.0 (L. Ding et al., 2020)
HCO_3^- Bicarbonate	1590 (Miao et al., 2016)	–	–
*CH_3 (methyl)	1470 (Yang et al., 2019)	1~3 (L. Ding et al., 2020)	20.9, 39.7 (L. Ding et al., 2020)
*HCOO- (formate)	2880 and 2965 (Yang et al., 2019)	–	–
*CH_2O	1378 and 1551 (Kusama et al., 1996)	–	–
*CHO (formyl)	1756 (Yang et al., 2019)	–	–
C-O in *OCH_3	1057 (Yang et al., 2019)	–	–
C—O—C stretch of dimethyl ether	1120 (Bahruji et al., 2022)	–	–
Adsorbed formate species, *HCOO	1742 (Arandia et al., 2023)	–	–
Bridging CO adsorption / CO/ ν(CO)	1918 (Panagiotopoulou, 2017)	–	–
Linearly adsorbed CO (CO_L)	2104 (Tountas et al., 2019)	–	–
Adsorbed *CO	2178 (Janke et al., 2014; Bacariza et al., 2019)	–	–
*CH_3O (methoxy)	2825 and 2927 (Yang et al., 2019)	–	60.7 (L. Ding et al., 2020)
CH_3COO*	3010 δ(CH), 1680 νas(OCO), 1511 νs(OCO) (L. Ding et al., 2020)	–	–

3. Catalysts for CO_2 methanation

CO_2 methanation is an exothermic reaction with a high kinetic barrier. A thermally stable catalyst with high resistance to coke formation is critical not only to increase the conversion and product selectivity but also to prevent deactivation at high temperatures and long reaction times. Designing an active catalyst for the reduction of CO_2 depends on several factors, such as the morphology of catalysts (Bian et al., 2018; Jomjaree et al., 2020), the size and dispersion of metal nanoparticles (M. C. Le et al., 2017), the presence of oxygen vacancies (F. Wang et al., 2016), the metal-support interactions (Quindimil et al., 2020; Ren et al., 2020), and the thermal and mechanical stability (Alrafei et al., 2020). The synthesis of a catalyst necessitates the selection of an active metal center for hydrogen dissociation, identifying catalyst support for CO_2 adsorption and dissociation, and, in some cases, adding a metal promoter for intermediate species stabilization. Ideally, the synthesis method should produce catalysts with the most active sites and metal/support interfacial contact. Another aspect of CO_2 methanation is reaction conditions, such as space velocity, temperature, pressure, and the type of reactor.

Ni is the most investigated catalyst for CO_2 methanation (Martínez et al., 2019; Pastor-Pérez et al., 2018). Apart from Ni, noble metals, such as Rh, Ir, and Ru were also investigated for CO_2 methanation (Table 3) (Aziz et al., 2014). Generally, Group VIIIB metals such as Ni, Co, Ru, and Rh were widely used as catalysts for CO_2 methanation. However, due to the high cost of noble metals, using Ru and Rh as catalysts is less attractive for commercialization. Other metals such as Pd, Pt, Mo, Ag, and Au exhibited CO_2 conversion into CH_3OH and CO, reducing CH_4

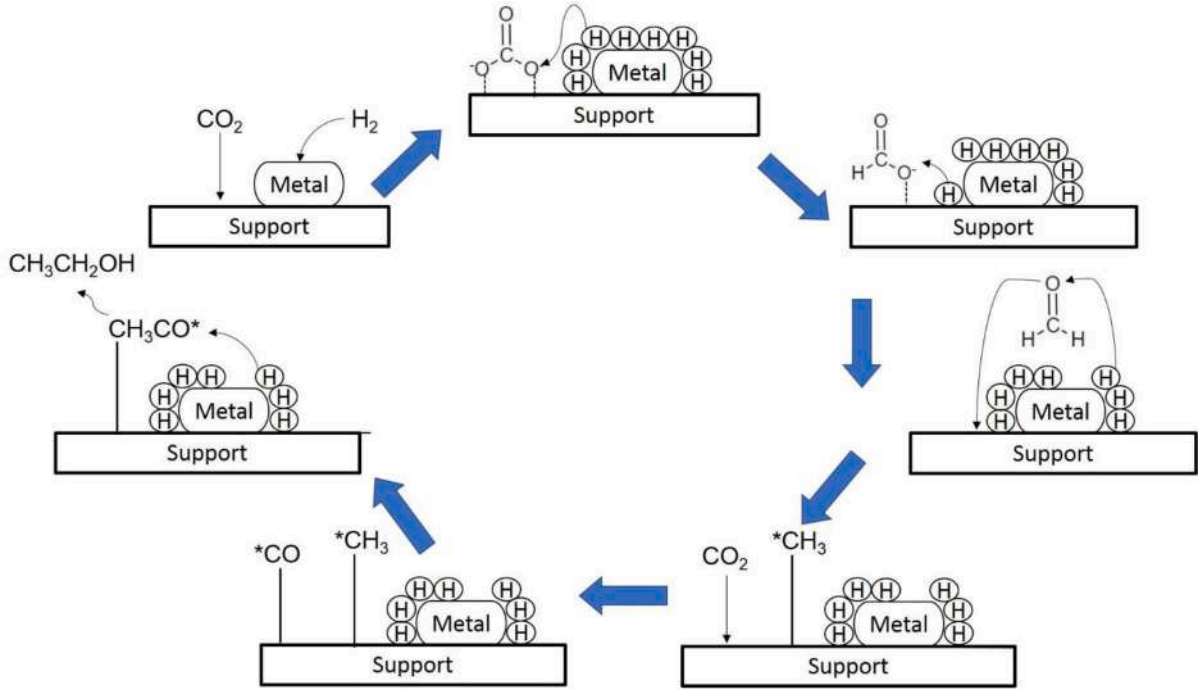

Fig. 7. Proposed mechanism of C—C coupling reaction in CO_2 hydrogenation to higher carbon molecules.

Table 3
The activity of metal-based catalyst on various supports for CO_2 methanation.

Catalysts	Synthesis	T (°C)	X_{CO2} (%)	S_{CH4} (%)	Ref
10%Ni/Al_2O_3	Coating	300 °C, 1 atm	83	90	(Fukuhara et al., 2017)
15%Ni/Al_2O_3	Co-precipitation	300 °C, 1 atm	16	48	(Frusteri et al., 2017)
60%Ni/Al_2O_3	Co-precipitation	300 °C, 1 atm	20	64	
15%Ni/Al_2O_3	Incipient wetness impregnation	300 °C, 1 atm	5	99	(Atzori et al., 2017)
10%Ni/SiO_2	Co-precipitation	300 °C, 1 atm	75	96	(T.A. Le et al., 2017)
10%Ni/ZrO_2	Co-precipitation	300 °C, 1 atm	85	80	
10%Ni/TiO_2	Co-precipitation	300 °C, 1 atm	18	18	
5%Ni/Zeolit-5A	Impregnation	300 °C, 1 atm	86	100	(Delmelle et al., 2016)
5%Ni/Zeolit-13X	Impregnation	300 °C, 1 atm	78	100	
15%Ni/USY	Impregnation	450 °C, 1 atm	70	100	(Bacariza et al., 2017)
14%Ni/HNaUSY	Impregnation	400 °C, 1 atm	65.5	94.2	(Graça et al., 2014)
15%Ni/USY zeolit	Impregnation	450 °C, 1 atm	80	100	(Bacariza et al., 2018)
15%Ni/MCM-41	Impregnation	450 °C, 1 atm	70	100	
15%Ni/SBA-15	Impregnation	450 °C, 1 atm	75	100	
5%Ni/ZSM-11	Impregnation	250 °C, 1 atm	65	30	(Azzolina-Jury et al., 2017)
2.5%Ni/ZSM-11	Impregnation	250 °C, 1 atm	60	30	
< 10%Ni/SBA-15	Hydrothermal	550 °C, 1 atm	78	100	(Liu and Tian, 2017)
Ni/MSN	Sol-gel	350 °C, 1 atm	0.3	0	(Aziz et al., 2014)
5%Rh/MSN	Impregnation	350 °C, 1 atm	99.5	100	
5%Ru/MSN	Impregnation	350 °C, 1 atm	95.7	100	
5%Ni/MSN	Impregnation	350 °C, 1 atm	85.4	99.9	
5%Ir/MSN	Impregnation	350 °C, 1 atm	9.5	83	
5%%Fe/MSN	Impregnation	350 °C, 1 atm	4	92	
5%Cu/MSN	Impregnation	350 °C, 1 atm	3.3	79	
3.7%Ru/CeO_2/r	Hydrothermal for CeO_2, followed by wetness impregnation	350 °C, 1 atm	75	99	(Ashok et al., 2020)
10%Ni/CeO_2	Wet impregnation	350 °C, 1 atm	93	100	
10%Ni/CeO_2-ZrO_2	Ammonia evaporation	275 °C, 1 atm	55	99.8	
10%Co/ZrO_2	Wetness impregnation	400 °C, 30 atm	92.5	99.9	
2%Co/ZrO_2	Incipient wetness impregnation	400 °C, 30 atm	85	99	
20%Co/KIT-6	Wetness impregnation	280 °C, 1 atm	48.9	100	

selectivity (Bahruji et al., 2016; Gutterød et al., 2020; Vourros et al., 2017; Geng et al., 2020). The advantages and drawbacks of several metals as CO_2 methanation catalysts are summarized in Table 4. The catalytic activities of metals were reported in the following orders (Jalama, 2017).

Ru> Rh> Ni> Fe> Co> Os> *Pt*> Ir> Mo> *Pd*> Ag> Au

Meanwhile, the order of selectivity for the catalysts is as follows:

Pd> *Pt*> Ir> Ni> Rh> Co> Fe> Ru> Mo> Ag> Au

Apart from the active metal catalyst, different supports have also been investigated, such as Al_2O_3, SiO_2, ZrO_2, CeO_2, and mixed oxides of Ce-Zr and TiO_2, primarily to enhance metal dispersion and promote CO_2 adsorption. High CO_2 adsorption on CeO_2 surface and the partial

Table 4
Comparison of metal catalysts for CO_2 methanation (Aziz et al., 2014; Jalama, 2017).

Metal based catalyst	Strength	Drawbacks
Rhodium (Ru)	Most active metal High methane yield at low temperature Higher stability than Ni	More expensive than Ni
Nickel (Ni)	Selective to CO and CH_4 Good activity performance maximum at 600 °C	Easily deactivated
Cobalt (Co)	Almost like Ni Does not need promoter	Higher prices compared to Ni
Iron (Fe)	Long lifetime catalyst Can be operated in higher temperature 700–950 °C	Very low activity
Molybdenum (Mo)	Higher methane selectivity than Ni Has sulfur tolerant	Low CO_2 conversion compared to Ni, Ru, Fe and Co

reduction of CeO_2 enhanced CO_2 conversion over Ni/CeO_2. Metal oxide CeO_2 with diverse morphologies, exposing different facets, resulted in high CO_2 conversion. When compared to octahedral and cubic shape CeO_2, well-controlled CeO_2 in a specific rod shape with 1 1 1 and 1 0 0 orientation increased catalytic activity by up to 80% conversion (Sakpal and Lefferts, 2018). Ni metal showed different catalytic activity when deposited onto MCM-41, HY, SiO_2 and γ-Al_2O_3. High concentrations of basic sites increased the turnover frequency, while defect sites or oxygen vacancies were responsible for the formation of surface carbon species (Aziz et al., 2015). High surface areas of the support enhanced Ni dispersion and crystal defects that can promote CO_2 conversion at low temperatures (Tada et al., 2017).

A metal promoter is incorporated into the CO_2 methanation catalyst to enhance selectivity and prevent catalyst deactivation (Table 5). The promoter was reported to enhance surface hydroxyl (-OH) groups and surface oxygen vacancies on support, which is crucial for promoting CO_2 adsorption and dissociation (Quindimil et al., 2018). For example, when non-reducible supports like Al_2O_3 and ZrO_2 were used, the presence of a metal oxide promoter like CeO_2 increased the number of oxygen vacancies, which improved CO_2 adsorption and dissociation (Pastor-Pérez et al., 2018). Similar trends in Ce when incorporated into a transition metal oxide support such as TiO_2 (Makdee et al., 2020). This section will elucidate the role of promoters such as Ce, rare-earth elements (La, Sm, and Gd), and alkali metal promoter (Li, Na, Ca, and K) for increasing the activity of Ni based catalysts.

3.1. Ce promoter

Cerium, as a promoter enhances the surface oxygen vacancy of the support (Makdee et al., 2020; Sun et al., 2020), improves Ni dispersion, prevents Ni sintering (Makdee et al., 2020; Hu and Lu, 2009; Gac et al., 2019; Guilera et al., 2019), increases the reducibility of Ni (Makdee et al., 2020; Guilera et al., 2019) and enhances CO_2 adsorption capacity (M.C. Le et al., 2017). Ceria (CeO_2) is generally used as support for CO_2 methanation catalysts and also in a variety of applications such as direct-methane fuel (Lda et al., 1999), FCC catalyst (Dejhosseini et al., 2013), CO oxidation, photocatalysis, and water-gas-shift (WGS) reactions (Vecchietti et al., 2014). CeO enhanced the adsorption and activation of oxygen-containing compounds, such as NO_x, CO_2, CO, and hydrocarbons. As a rare-earth element, the utilization of Ce for support is not economically viable due to its high price. Therefore, Ce was used in a small quantity to promote the number of surface oxygen vacancies Al_2O_3 and TiO_2 (Guilera et al., 2019; Liu et al., 2012). On reducible supports such as TiO_2, Ce altered the structural properties of the support, which consequently enhanced CO_2 methanation. EXAFS analysis revealed the expansion of the TiO_2 lattice due to Ce incorporation into the TiO_2 lattices, which was responsible for the generation of oxygen vacancies (Makdee et al., 2020).

Ce improves metal-support interaction and reducibility when used as a promoter on non-reducible supports, such as Al_2O_3 and zeolite. As non-reducible supports, the number of oxygen vacancies of Al_2O_3 and zeolite was limited; therefore, incorporation of Ce increased Ni reducibility through the oxygen mobility properties of CeO_2. Ce also introduced the intermediate strength basic sites that can promote CO_2 adsorption and

Table 5
Metal promoter for Ni-based catalysts in CO_2 methanation reaction.

Promoter	Catalyst	Surface area (m^2/g)	Catalytic activity		Promoter content (%wt)	X_{CO2} (%)	S_{CH4} (%)	Ref.
			T (°C)	H_2/CO_2				
–	Ru/TiO_2	–	450	4/1	–	50	80	(Petala and Panagiotopoulou, 2018)
Cs	Ru/TiO_2	–	450	4/1	0.2	62	96	
K	Ru/TiO_2	–	450	4/1	0.2	60	84	
Li	Ru/TiO_2	–	450	4/1	0.2	60	81	
Na	Ru/TiO_2	–	450	4/1	0.2	65	97	
Na	Ru/TiO_2	–	450	4/1	0.4	69	98	
Na	Ru/TiO_2	–	450	4/1	0.6	70	99	
–	Ni/ZrO_2-V	89.45	450	4/1	–	70	88	(Lu et al., 2016)
La	Ni/ZrO_2-V	73.78	450	4/1	0.83	89	85	
Fe	Ni/ZrO_2-V	74.28	450	4/1	2.93	75	95	
Ce	Ni/ZrO_2-V	75.99	450	4/1	1.39	79	85	
Co	Ni/ZrO_2-V	74.71	450	4/1	1.15	74	90	
Ce-Pr	Al_2O_3/SiO_2	128.6	400	4/1	4	40	83	(Lechkar et al., 2018)
Ce-Pr	Al_2O_3/SiO_2	141.9	400	4/1	1.5	35	80	
Ce-Pr	5%wt Ni/Al_2O_3/SiO_2	142.9	350	4/1	4	55	99	
Ce-Pr	5%wt Ni/Al_2O_3/SiO_2	131.9	350	4/1	1.5	49	90	

hydrogenation (Debek et al., 2015). Apart from enhancing the dispersion of Ni and Ni-Al_2O_3 interactions, incorporation with Ce also exhibited a higher CO_2 adsorption capacity (Daroughegi et al., 2021). Nizio et al. (Nizio et al., 2016) used Ce as promoters for Ni-Mg-Al hydrotalcite-derived catalysts, indicating high activity following the addition of Ce promoter at relatively higher temperatures. The role of Ce as a promoter of nickel catalysts was also compared to La, Fe, and Co using zirconia modified clays as support. The catalysts doped with rare earth La and Ce exhibited higher methane selectivity than those doped with transition metals Fe and Co. The reduction of Ce^{3+} to Ce^{4+}produces defects and promotes the generation of oxygen vacancies to facilitate direct dissociated adsorption for CO_2 conversion (Lu et al., 2016).

3.2. Other rare earth element promoters

Other rare earth elements such as La, Sm, Y, and Gd have been investigated as Ni promoters mainly to enhance the basicity of the catalysts (Li et al., 2005). The number of basic sites increased in general with promoter loading (Wierzbicki et al., 2016). The evolution of lanthanum oxide has been shown to cause partial blockage of hydrotalcites basic sites and to introduce a new medium-strength basic site (D. Wierzbicki et al., 2018). CO_2-TPD profiles of La-derived catalysts indicated three deconvoluted Gaussian peaks corresponding to low strength basic sites (surface OH^-), medium, and strong (low-coordination surface O^{2-}). The additional medium strength basic sites were known to play a role in the CO_2 methanation reaction. Aside from improving catalyst basicity, rare-earth promoters improved Ni dispersion, lowering Ni activation energy, and preventing Ni deactivation (Xu et al., 2017; Perkas et al., 2009). Most Ni catalysts interacted strongly with support, necessitating a high temperature reduction, which is not ideal for low temperature reactions. For example, Ni deposited on Al_2O_3 showed a strong interaction as the result of the formation of the hard-reducible nickel aluminate species (Vrijburg et al., 2020; Cai et al., 2011). Since CO_2 methanation favours reactions at low temperatures, promoters were added to control the metal/support interaction. Lanthanum oxide reduced the interaction between Ni and the Al-Mg hydrotalcite matrix, resulting in improved reducibility (D. Wierzbicki et al., 2018). Another investigation on La, Zr, Fe, Co, and Cu as promoters on Ni/Al_2O_3 catalysts showed the potential of rare-earth elements to increase Ni reducibility, stability, and catalytic performance at low temperatures (Valinejad Moghaddam et al., 2018). Methods for incorporation of metal promoters La was also explored via co-precipitation, impregnation, and ion-exchange on a Ni-hydrotalcite based catalyst. The ion-exchange method produced catalysts with increased basic sites, while the impregnation led to the reduction of medium strength basic sites. The results showed outstanding catalytic activity at 300 °C, with CO_2 conversions around 36–87% and CH_4 selectivity of 98–99% at low temperatures around 250 °C (D. Wierzbicki et al., 2018).

Gadolinum doped ceria (GDC) has been investigated as a support for CO_2 methanation (Vita et al., 2018). The presence of Gd_2O_3 as a promoter enhanced the structural properties of Ni/CeO_2 catalysts, such as crystallite size, surface area, metal-to-support interaction, basicity, and oxygen vacancies, and improved thermal and mechanical resistance (Vita et al., 2018). Frontera et al. (Frontera et al., 2017) also reported the formation of catalysts with enhanced dispersion of Ni nanoparticles when using GDC as support. The catalysts also showed a strong Ni-Ce interaction that evidently improved CO_2 conversion (>90%) at 400 °C with almost 100% selectivity to CH_4.

Rare-earth element as promoter enhanced the surface oxygen vacancy of catalysts as reported on Sm and Y on Ni/ZrO_2 (Takano et al., 2011). Ni/*Sm/Zr*O_2 produced from an aqueous ZrO_2 solution containing nickel and rare earth element salts at 50% Ni and 50% Zr-Sm oxide loading demonstrated enhanced methanation activity (Takano et al., 2011). The oxygen vacancies that were created following the introduction of Sm and Y promoters formed a strong interaction between support and oxygen in CO_2, thus weakening the C–O bond strength and leading to the enhancement of hydrogenation of CO_2 to form CH_4. Yttrium (Y) was also reported to exist as Y^{3+} as an important species for CH_4 formation due to the adsorption of CO_2 on oxygen vacancy sites (Takano et al., 2016).

3.3. Alkali and alkali earth metals promoter

Alkali and alkali earth metals such as Li, Na, K and Ca were utilized as promoters mainly to improve the oxygen vacancies, Ni dispersion and to control the formation of intermediates to favor methane production. The addition of Na to Ni/SiO_2 via the wet impregnation method at various concentrations reduced the size of Ni nanoparticles. Na was observed near Ni, thus preventing particle agglomeration by blocking the surface of metallic Ni. The results showed high activity of Na/Ni/SiO_2 to give 90% of CO_2 conversion for 10 h (Le et al., 2018). Takano et al. (Takano et al., 2015) synthesized Ni/Ca-doped ZrO_2 catalysts with varying Ca^{2+} concentrations and found that increasing Ca^{2+} concentration increased catalytic activity for CO_2 methanation. Ni/Ca-doped ZrO_2 catalysts also achieved almost 100% CH_4 selectivity. Ca and Ni existed as ions that were incorporated within tetragonal ZrO_2, thus creating oxygen vacancies (Eq. (19) and Eq. (20)).

$$CaO = Ca_{Zr} + V_o + O_o \tag{19}$$

$$NiO = Ni_{Zr} + V_o + O_o \tag{20}$$

The oxygen vacancies attracted CO_2 to form intermediate carbonate species on the ZrO_2 surface. Atomic hydrogen on Ni particles progressively reduced the adsorbed carbonate species into formate, formaldehyde, methoxy, and methane. A comparison of the effects of various alkali promoters (Li, Na, K, and Cs) at different weight loadings (0.0–0.40 wt.%) on Ru/TiO_2 catalysts was carried out by Petala et al. (Petala and Panagiotopoulou, 2018). Turnover frequency (TOF) of promoted 0.5%Ru/TiO_2 catalysts follows the order of TiO_2 (unpromoted) < Li ~ K < Cs < Na. Alkali promoters were suggested to improve the hydrogenation of intermediates for CH_4 formation over well dispersed Ru particles. The optimized 0.5%Ru/ 0.2%Na-TiO_2 catalyst exhibited a higher specific activity than 5% Ru loading, therefore, is a promising candidate for the CO_2 methanation reaction.

4. Catalysts for CO_2 hydrogenation to C_{2+} products

CO_2 hydrogenation towards higher hydrocarbons or alcohols is a thermodynamically challenging process due to the further C—C coupling reaction required for carbon chain growth. Therefore, the reaction is generally carried out at high pressure to overcome thermodynamic restrictions. The stoichiometric CO_2 to hydrogen ratio in the methanation reaction is fixed at 1:4; however, for higher hydrocarbon products, the amount of hydrogen gasses varies depending on the desired products (Dorner et al., 2009; Wei et al., 2017). Most of the reported studies, as summarized in Tables 6 and 7, have variable ratios of CO_2:H_2 from 1:1 to 1:6, with the different concentrations of gas reactants affecting the selectivity of hydrocarbons. Hydrogenation of CH_3* intermediates into CH_4 was inhibited when the CO_2 to H_2 gas feed ratio was reduced from 1:4 to 1:3 (Dorner et al., 2009). Nevertheless, the reaction can be summarized below for ethylene and ethanol formation (Eq. (21) and Eq. (22)).

$$2\ CO_2 + 6\ H_2 \rightarrow CH_3CH_2OH + 3\ H_2O \tag{21}$$

$$2\ CO_2 + 6\ H_2 \rightarrow C_2H_4 + 4\ H_2O \tag{22}$$

In CO_2 hydrogenation to higher hydrocarbons or alcohol, the catalysts must possess an active center that can stabilize CO* or CH_x* intermediates for the C—C coupling reaction (Ye et al., 2020; L. Wang et al., 2018). The formation of methyl (CH_3*) and CO* species was crucial in promoting the C—C coupling reaction for forming longer chain molecules. CO_2 methanation catalysts or hydrogenation catalysts

Table 6
Catalysts for CO_2 hydrogenation to light olefin.

Catalysts	Promoter	Preparation	Reaction condition	Conversion	Ref.
CuCe/SAPO-4	Ce	Deposition-precipitation	T = 300–500 °C P = 2MPa $3H_2$:CO_2	χCO_2= Solefin=70.4%	(Sedighi and Mohammadi, 2020)
$Fe_{0.30}Co_{0.15}Zr_{0.45}K_{0.10}O_{1.63}$	K	Hydrothemal synthesis	Fixed bed reactor T = 260–250 °C P = 2MPa $4H_2$:CO_2 LHSV: 3500 h^{-1}	χCO_2= 63.98% SC_2H_4=63%	(Ding et al., 2019)
Mn–Na/Fe	Na	co-precipitation method	stainless steel tubular (i.d. 10 mm) fixed-bed reactor T = 260–250 °C P = 3MPa Feed gas H_2/CO_2/Ar =of 69/23/8/1 GHSV: 2040 mL h^{-1} $gcat^{-1}$	χCO_2= 38.6% SC_2–C_4=30.2%	(B. Liang et al., 2019)
Na-$CoFe_2O_4$/CNT	Na	thermal decomposition of a metal–oleate complex	stainless steel fixed-bed reactor T = 260–250 °C P = 1MPa Feed gas $H_2/CO_2/N_2$ = 9/3/1 WHSV=3600 $mL.^{h-1}.gcat^{-1}$	χCO_2= 34.4% $SC_2^=$-$C_4^=$=38.8%	(Kim et al., 2020)
Carburized ceramic K/FeAl-O nanobelts	K	Electrospinning	stainless steel fixed-bed reactor T = 300 °C P = 1MPa Feed gas H_2/CO_2 = 4/1 WHSVCO_2 = 1 h^{-1}	χCO_2= 48% $SC_2^=$-$C_4^=$=52%	(Elishav et al., 2020)
Fe-Co/K-Al_2O_3	K	two-step incipient wetness impregnation method	fixed bed stainless steel reactor T = 300 °C P = 2MPa Feed gas $H_2/CO_2/N_2$ = 3/1/1	χCO_2= 49% $S_{hydrocarbon}$= 90.6% Olefin/ paraffin=6.5	(Numpilai et al., 2017)

were modified with promoters to control the ability to adsorb and dissociate H_2, thereby limiting methane formation. Apart from that, promoters such as Co and Mn, and alkali metal promoters such as Na and K enhanced surface hydroxyl and oxygen vacancies to initiate C—O bond dissociation (Ding et al., 2019; B. Liang et al., 2019). Another popular method for producing higher hydrocarbons is through the formation of hybrid bifunctional catalysts. Hybrid $CuCeO_2$/SAPO-4 catalysts increased the conversion of CO_2 to light olefin at high temperatures. CO_2 hydrogenation to a longer chain molecule was carried out at 400 °C, above the ideal temperature for methanol synthesis. The resulting CO was then reacted with methoxy species to produce olefin (Sedighi and Mohammadi, 2020).

4.1. *Promoter for CO_2 hydrogenation to olefin*

The mechanism of CO_2 hydrogenation to olefin discussed in Section 2.2 illustrated the importance of controlling the formation of CH_3* species for C—C coupling. Further hydrogenation of CH_3* produced methane, thus reducing selectivity towards C_2 molecules. Promoter enhances the number of surface oxygen vacancies for C—O bond dissociation and reduces the hydrogenation potential, preventing methane formation. Metal oxide promoters such as Co and Mn were added to create synergy with Fe and consequently influence H_2 dissociation ability (Z. Zhang et al., 2020). Interaction between iron as an active species with another metal oxide promoter, such as Co, reduced the interaction with adsorbed H_2 (Satthawong et al., 2015). As a metal promoter, potassium (K) partially covered the metal surface with its oxide, reducing the adsorption strength with hydrogen and, as a result, restricting further hydrogenation (Satthawong et al., 2015). CO_2 hydrogenation to olefin is under competition with paraffin formation (Z. Zhang et al., 2020). Controlling the hydrogenation potential of the catalysts suppressed paraffin formation. Na and Mn promoters were reported to enhance selectivity towards olefin when added to Fe_3O_4 catalysts (Z. Zhang et al., 2020). The spatial hindrance of Mn suppresses the chain growth, consequently enhancing the number of surface short alkyl-metal intermediates. The synergy created with the Na promoter that could transfer electrons from Na to Fe atoms favors the beta-H abstraction of the short alkyl-metal intermediates to form light olefin. The electron transfer between Na and Fe atoms allowed back donation to C* in the C-metal bond (Liu et al., 2018).

Most of the investigated metal catalysts for CO_2 hydrogenation to olefin are Fe and Cu deposited on supports such as ZrO_2 (Gu et al., 2019; J. Ding et al., 2020), zeolite (Sedighi and Mohammadi, 2020; Huang et al., 1995), and Al_2O_3 (W. Wang et al., 2018; Satthawong et al., 2015). Bifunctional nanostructured catalysts with high oxygen vacancies were formed on $Fe_xCo_yZr_zK_pO_\delta$ catalysts. Oxygen vacancies facilitated CO_2 dissociation into CO as an intermediate species for the C—C coupling reaction and inhibited CH_4 by-products (Le et al., 2018). Oxygen vacancies can stabilize the intermediates in CO_2 hydrogenation and activate the CO_2 via adsorbing the O atoms in CO_2 molecule (Gu et al., 2019; Hamid et al., 2017). The addition of Mn as a promoter on Na/Fe catalysts appeared in close proximity to Fe species, controlling the capacity and strength of CO adsorption for further C—C coupling to longer chain olefins (B. Liang et al., 2019). Mn was also responsible for the formation of Fe_5C_2 active species that is responsible for producing hydrocarbon and inhibiting the RWGS reaction on Fe_3O_4. The optimized loading of Mn enhanced Fe_5C_2 formation and consequently reduced the carbon chain growth, selectively producing C_2–C_4 hydrocarbons (B. Liang et al., 2019).

The interfacial contact between carbonaceous potassium, K promoters, and iron catalysts allowed for precise control of C—O dissociation and subsequent C—C coupling for high yields of hydrocarbon olefins (Han et al., 2020). Utilization of carbonaceous K promoted the interaction between K_2CO_3 and active Fe_5C_2 species, as evident by HRTEM analysis (Han et al., 2020). A bimetallic alloy carbide ($Fe_{1-x}Co_x)_5C_2$ formation in Na-$CoFe_2O_4$/CNT was identified as an active catalytic site for CO_2 hydrogenation towards the preferential C_2–C_4 olefins (Kim et al., 2020). The advantages of carbide species toward carbon chain formation were also observed on K/Fe-Al-O spinel catalysts. Carbide species were purposefully produced at 300 °C under CO/H_2 flow to ensure high CO_2 conversion and selectivity to light olefins (Elishav et al., 2020). Improving CO_2 hydrogenation to light olefin is by increasing the interaction between the metal oxide and K promoter. An investigation into the structural changes of Fe-Co/K-Al_2O_3 catalysts when calcined at

Table 7
Catalysts for CO_2 hydrogenation to ethanol/alcohol.

Catalyst	Promoter	Preparation	Reaction condition	Conversion	Active sites	Ref.
Cs-Cu-Fe-Zn	Cs	Impregnation	Fixed-bed reactor $T = 350$ °C $P = 5.0$ MPa	STY etanol of 73.4 mg $gcat^{-1}h^{-1}$	CuFeZn	(Xu et al., 2020)
K-Mn-Fe_2O_3/N—CNT	K-Mn	Impregnation	Fixed-bed reactor $T = 653$ K $P = 25$ bar	Xco_2=34.39 $S_{alcohol}$=70.5	Fe_2O_3	(Kangvansura et al., 2017)
Na-Co/SiO_2	Na	Incipient wetness impregnation	Flow reactor $T = 250$ °C $P = 5.0$MPa $3H_2$:CO_2 GHSC=4000 h^{-1}	Xco_2=18.82 $S_{alcohol}$=9.54 $S_{ethanol/alcohol}$ = 62.81	Co_2C	(S. Zhang et al., 2020)
PdCu/TiO_2	Pd	Colloidal method	Stainless steel autoclave $T = 200$ °C $P = 3.2$ MPa $3H_2$:CO_2	Xco_2= N.D $S_{alcohol}$=*N*.D $S_{ethanol/alcohol}$ = 78.1%	Pd_2C	(Bai et al., 2017)
Au/TiO_2	–	Deposition-precipitation	Stainless steel autoclave $T = 200$ °C $P = 50$ bar $3H_2$:CO_2 Solvent: DMF	STY= 942.8 mmol gAu −1 *h* − 1,	Anatase oxygen vacancies	(D. Wang et al., 2016)
RhFeLi/TiO_2	Rh-Fe	Impregnation	Fixed bed microreactor $T = 200$ °C $P = 30$ bar $3H_2$:CO_2	Xco_2= 15% $S_{ethanol}$=30% Ethanol yield = 5%	Hydroxyl group	(Yang et al., 2019)
$CoAlO_x$	–	Precipitation with urea	Stainless steel autoclave $T = 200$ °C $P = 4$ MPa $3H_2$:CO_2	Ethanol yield = 0.892 mmol gcat −1 h −1 . $S_{ethanol}$ = 88.9%	Co-CoO metal-metal oxides composition	(L. Wang et al., 2018)
Pd/Fe_3O_4	–	Deposition and reduction with $NaBH_4$	Packed bed reactor $T = 250$ °C, $P = 20$ bar $3H_2$:CO_2	Xco_2= 1.4% $S_{ethanol}$=98% Ethanol yield = 440 mmol/gPd.h	Pd single atom	(Caparrós et al., 2018)
$CoNiAlO_x$	–	Co-precipitation	Stainless stees autoclave $T = 250$ °C, $P = 4$MPa $3H_2$:CO_2	$S_{ethanol}$= 85.7% Ethanol yield = 15.8 mmol $gcat^{-1}$	CoNi alloy phase	(Wang et al., 2019)
Co/La-Ga-O	La	Citrate-complexing method	Fixed-bed flow micro-reactor. $T = 240$ °C, $P = 3$MPa $3H_2$:CO_2, GHSV= 3000 mL/(gcat)	Xco_2= 9.8% $S_{ethanol}$=74.7%	Co^0 and $Co^{\delta+}$	(Zheng et al., 2019)
Ir-In_2O_3	–	Wet impregnation	stainless-steel autoclave 1 MPa of CO_2 and 5 MPa of H_2 $T = 200$ °C	$S_{ethanol}$=99.7% TOF = 481 *h* − 1	Ir single atom	(Majhi et al., 2019)
Rh-Li/SiO_2	Li	Wet impregnation	Stainless stees autoclave $T = 513$ K, $P = 5$MPa $3H_2$:CO_2, 100 ml/min	Xco_2= 7% $S_{ethanol}$=15.5%	Li stabilize CO as intermediate species	(Kusama et al., 1996)

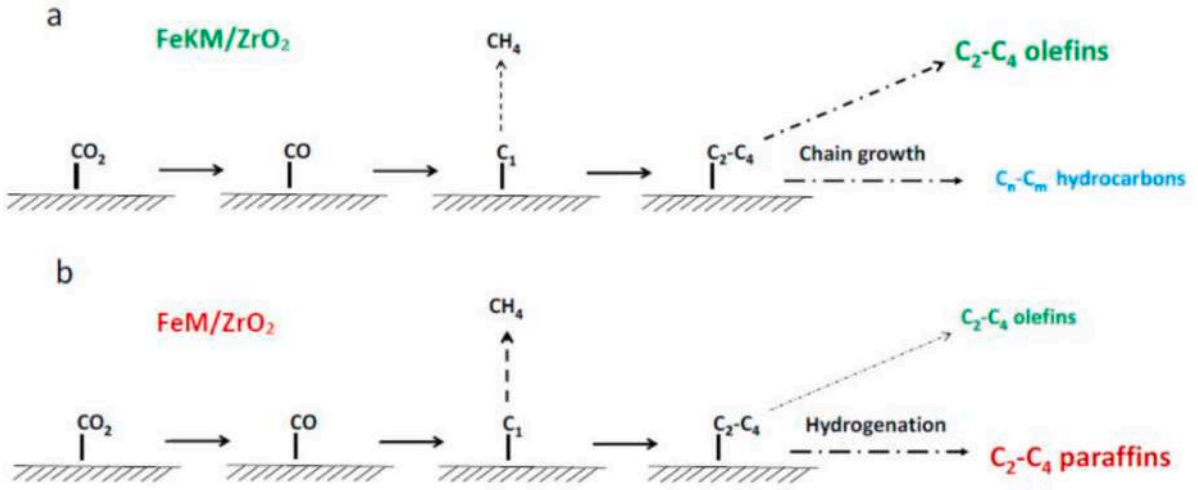

Fig. 8. CO_2 hydrogenation to olefin a) with K promoter and b) without promoter (Barrios et al., 2022). Copyright © 2022 American Chemical Society.

various reaction temperatures revealed physicochemical changes in the catalysts and metal oxide interaction (Numpilai et al., 2017). K was also reported to enhance CO_2 adsorption capacity on Fe-CO catalysts (Satthawong et al., 2015).

A well dispersed Mn promoter on a Fe_3O_4 catalyst was reported to enhance CO_2 adsorption and activation of C = O bonds. Mn inhibits secondary hydrogenation reaction, consequently improving the olefin selectivity. Increasing Mn concentration reduced paraffin production without affecting the conversion or CH_4 selectivity, suggesting Mn inhibited further hydrogenation of olefin to paraffin (Jiang et al., 2020). Mn and K were also used as promoters to boost the activity of iron catalysts deposited onto nitrogen-doped carbon nanotubes (Kangvansura et al., 2017). Another study on the effect of Mn promoter on NaFe catalysts indicated that the tuning of Mn content affected the physicochemical properties of iron oxides. A high loading of Mn produced the formation of surface Fe species around Mn that enhanced CO_2 adsorption. However, the Fe_5C_2 species required for CO hydrogenation to hydrocarbon was increased in low Mn concentrations (Z. Zhang et al., 2020). The importance of Fe_5C_2 species in converting CO to hydrocarbons was further reported on Na promoter. The presence of Na suppressed methane production due to the formation of Fe_5C_2 species that depended on Na concentration (B. Liang et al., 2019).

Barrios et al. (2022) categorized the role of K (Fig. 8) as structural and electronic promoters. Structural promoters typically increase iron dispersion and carbidization, improving mechanical resistance. Electronic promoters improve the intrinsic activity of active sites (TOF). The promotion of alkaline metals decreases the ability of the catalyst to hydrogenate and enhances the rate of oligomerization of C_1 surface monomers. Thus, oligomerization limits the light olefin selectivity of catalysts containing alkaline metals, while the contributions of the hydrogenation of the adsorbed C_2–C_4 species and the secondary hydrogenation of light olefins are negligible. This shows that surface oligomerization should be inhibited following the creation of C_4 surface fragments to improve the light olefin selectivity of catalysts boosted with alkaline metals.

4.2. Promoter for CO_2 hydrogenation to ethanol

CO_2 hydrogenation to ethanol was largely investigated using noble metals such as Rh (Yang et al., 2019; Kusama et al., 1997; Erdőhelyi, 2020), Pd (Bai et al., 2017; Caparrós et al., 2018), and Au as catalysts (D. Wang et al., 2016) with single atom orientation. A single Pd atom anchored on the Fe_3O_4 surface showed high activity for ethanol production. Under reducing conditions, specific metal-support interaction created oxygen vacancies and interstitial sites on Fe_3O_4, forming a specific active site between a Pd single atom and Fe_3O_4 to initiate C—C coupling. The metal and surface interaction was not observed using ZrO_2 and CeO_2 supports (Caparrós et al., 2018). Ir catalysts are another noble metal that has been studied for CO_2 hydrogenation to ethanol. Ir-In_2O_3 single atom catalysts were produced using wet impregnation of H_2IrCl_6 solution on In_2O_3. The catalyst exhibited high selectivity toward ethanol, at 99% selectivity during liquid hydrogenation of CO_2. C—C bond coupling occurred between CO* generated on the isolated Ir atom species and adsorbed CH_3O* on In_2O_3. Lewis acid-base pair formed between the single atom Ir and the adjacent oxygen vacancy in In_2O_3 promoted C—C coupling to form ethanol (Majhi et al., 2019).

The limitation of single atom catalysts for CO_2 hydrogenation to ethanol is their susceptibility to particle sintering, especially when the reaction time is long, and the temperature is high. The addition of a secondary metal promoter, such as Cu, formed a bimetallic Pd alloy that guided CO_2 hydrogenation towards C—C coupling to ethanol (Bai et al., 2017). In CO_2 hydrogenation to ethanol, a Pd_2Cu bimetallic catalyst deposited on TiO_2 improved selectivity, stability, and activity. Pd-Cu charge transfer enabled CO_2 hydrogenation to ethanol, which was previously restricted to Pd monometallic (Bai et al., 2017). In the presence of a Ga promoter, high ethanol production was observed via a physical mixture of Pd and Ga on Fe-based FT catalysts due to the suppression of hydrogen spillover and the reduction of the amount of exposed Fe that inhibited the methanation reaction. Pd and Ga concentrations were varied to maintain the optimum oxidation–reduction states of FT catalysts for ethanol production (Inui et al., 1999).

The presence of surface oxygen vacancies was also reported as an essential aspect of catalysts for ethanol production. Au nanocluster deposited on TiO_2 showed abundant oxygen vacancies created on TiO_2 anatase, increasing the performance of ethanol at mild reaction conditions. The studies indicated that Au clusters on anatase showed superior ethanol formation compared to rutile, brookite, and amorphous TiO_2. The importance of oxygen vacancy was also reported when using Rh/TiO_2 catalysts. TiO_2 as support and a high concentration of hydroxyl groups created a synergistic effect with the well dispersed Rh nanoparticles to stabilize formate intermediates and protonated methanol. RhFeTi was deposited on TiO_2 prepared from the hydrothermal synthesis of a mixture of titanium tetrachloride, nitric acid, and water. The resulting TiO_2 showed a high concentration of hydroxyl groups compared to commercial TiO_2, reducing the energy barrier for C—O bond scission (Yang et al., 2019).

Adding metal promoters to noble metal catalysts reduced the hydrogenation potential. Rh/SiO_2 catalysts deposited with a Li promoter enhanced selectivity and CO_2 conversion to ethanol while constraining further hydrogenation of CO intermediate species to methane (Kusama et al., 1996). Fe promoter was also reported to increase selectivity towards ethanol on Rh catalysts by catalyzing CO formation from RWGS. However, high concentrations of Fe encapsulated in Rh can deactivate the catalyst (Yang et al., 2019). Apart from precious metal catalysts, transition metals such as Co, Cu and Fe have also received significant interest with promising activity to activate C—C coupling during CO_2 hydrogenation reaction to ethanol (L. Ding et al., 2020; Gogate and Davis, 2010; Zheng et al., 2019). In its oxidized states, Cobalt could form oxygen vacancies under a reducing environment that help dissociate CO_2 into CO intermediates. Cobalt was also used as support for noble metal catalysts to produce higher alcohol. Pt deposited on Co_3O_4 showed superior activity than Ru, Rh and Pd (He et al., 2016). However, the type of solvent significantly influenced the activity of Pt/Co_3O_4. Water enhanced ethanol production at low temperatures compared to (1, 3-dimethyl-2-imidazolidinone (DMI). Water facilitated the dissociation of methanol to form *CH_3 during C—C coupling reaction (He et al., 2016). $CoAlO_x$ catalysts produced from co-precipitation have high selectivity to ethanol following reduction at 600 °C. XANES analysis of the $CoAlO_x$ catalyst reduced at 600 °C indicated the formation of Co metallic co-existence with CoO, responsible for increasing the formation of CH_x* species for C—C coupling. The composition of Co-CoO_X was crucial for enhancing ethanol production on Cobalt based catalyst (L. Wang et al., 2018).

The oxidation states of Co are critical in navigating the selectivity towards ethanol. Co in its metallic state reduced CO_2 into methane, therefore modification of Co with metal promoter controlled its reduction potential to increase ethanol production. Cobalt catalysts promoted with Na deposited on SiO_2 and Si_2N_4 produced 18% CO_2 conversion, with 62.8% ethanol selectivity relative to the alcohol distribution at 250 °C and 5 MPa. The catalysts also produced CO and methane as byproducts of the reverse water gas shift and methanation reactions. The important parameters that influenced ethanol production were suggested to be originated from the strong metal-support interaction between Si-O-Co bond (S. Zhang et al., 2020). Co was incorporated with Ni metal to form $CoNiAlO_x$ catalysts to enhance CO_2 hydrogenation to ethanol while suppressing methane formation. The presence of CoNi phase accelerated the formation of *CH_x intermediate, the vital species that initiated C—C coupling (Wang et al., 2019). The advantage of suppressing Co metallic phase was further evidenced by incorporating the Ga promoter in Co/La-Ga-O composite. Although the CO_2 conversion was significantly reduced following Ga addition due to the inhibition of methane, the resulting products showed a high distribution

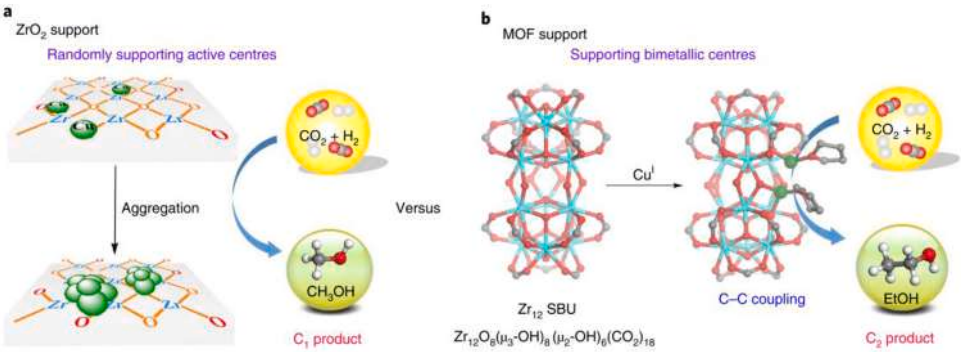

Fig. 9. Schematic illustration of Cu supported on ZrO_2 and MOF for CO_2 hydrogenation (An et al., 2019). Copyright © 2019 Nature Springer.

towards ethanol. The selectivity of ethanol was increased via the incorporation of Ga in proximity with Co. Ga suppressed the formation of methane and enhanced ethanol production. Ga also stabilized Co^0 to form a synergistic effect between Co^0 and $Co^{\delta+}$. The promotional effect of Ga was proven by the shift of H_2 TPR peak, which indicated Ga stabilized Co^{2+} species and prevented metallic Co° formation (Zheng et al., 2019). The effect of support on Cu activity was illustrated in Fig. 9.

5. Summary and future perspective

Hydrogenation of CO_2 to value added carbon commodities is a green route for utilization of the major greenhouse gas arising from anthropogenic activity. Apart from conversion to methane, a wide range of applications of long chain carbon molecules in industries has prompted studies towards the production of alcohol and olefin from CO_2. The structure of the catalysts and the reaction conditions significantly influenced the selectivity of hydrogenated molecules. Direct CO_2 hydrogenation to longer chain molecules such as olefin and ethanol required a high pressured catalytic reaction system compared to CO_2 methanation reaction. The major challenge for CO_2 hydrogenation reaction to higher carbon molecules is to increase C—C coupling reaction steps. This can be achieved by controlling further hydrogenation of CHx* intermediates species to CH_4. Retaining the C—O bond during C—C coupling step was proven to be a challenge. Based on the type of catalysts, the intermediate species that initiated C—C coupling reaction were determined as methyl species (*CH_3) and carbon monoxide species (*CO) that will react to form C—C bond. This review has highlighted that metal promoters are essential to control H_2 dissociation potential and CO_2 activation. Promoters modify metal catalyst reducibility, metal dispersion and thermal stability against coke deposition.

CRediT authorship contribution statement

Novia Amalia Sholeha: Conceptualization, Data curation, Writing – original draft. **Holilah Holilah:** Data curation, Visualization. **Hasliza Bahruji:** Supervision, Writing – review & editing, Funding acquisition. **Athirah Ayub:** Writing – review & editing. **Nurul Widiastuti:** Supervision, Writing – review & editing. **Ratna Ediati:** Writing – review & editing. **Aishah Abdul Jalil:** Supervision, Writing – review & editing. **Maria Ulfa:** Data curation, Writing – review & editing. **Nanang Masruchin:** Writing – review & editing. **Reva Edra Nugraha:** Data curation, Visualization. **Didik Prasetyoko:** Supervision, Writing – review & editing, Funding acquisition.

Declaration of Competing Interest

The authors declare that they have no known competing financial interests or personal relationships that could have appeared to influence the work reported in this paper.

Acknowledgements

The authors would like to acknowledge the support from the Ministries of Research, Technology, and Higher Education Republic of Indonesia under World Class Research (WCR) No. 1603/PKS/ITS/2022] and Universiti Brunei Darussalam FIC Research Grant (UBD/RSCH/1.9/FICBF(b)/2022/016) for funding this research.

References

Adegoke, K.A., Maxakato, N.W., 2022. Electrochemical CO_2 conversion to fuels on metal-free N-doped carbon-based materials: functionalities, mechanistic, and technoeconomic aspects. Mater. Today Chem. 24, 100838 https://doi.org/10.1016/j.mtchem.2022.100838.

Al-mamoori, A., Krishnamurthy, A., Rownaghi, A.A., Rezaei, F., 2017. Carbon capture and utilization update. Energy Technol 5, 834–849. https://doi.org/10.1002/ente.201600747.

Alrafei, B., Polaert, I., Ledoux, A., Azzolina-Jury, F., 2020. Remarkably stable and efficient Ni and Ni-Co catalysts for CO_2 methanation. Catal. Today. 346, 23–33. https://doi.org/10.1016/j.cattod.2019.03.026.

An, B., Li, Z., Song, Y., Zhang, J., Zeng, L., Wang, C., Lin, W., 2019. Cooperative copper centres in a metal–organic framework for selective conversion of CO_2 to ethanol. Nat. Catal. 2, 709–717. https://doi.org/10.1038/s41929-019-0308-5.

Arandia, A., Yim, J., Warraich, H., Lepp, E., Lempelto, A., Gell, L., Jiang, H., Meinander, K., Viinikainen, T., Huotari, S., Honkala, K., Puurunen, R.L., 2023. Effect of atomic layer deposited zinc promoter on the activity of copper-on-zirconia catalysts in the hydrogenation of carbon dioxide to methanol. Appl. Catal. B Environ. 321, 122046 https://doi.org/10.1016/j.apcatb.2022.122046.

Ashok, J., Pati, S., Hongmanorom, P., Tianxi, Z., Junmei, C., Kawi, S., 2020. A review of recent catalyst advances in CO_2 methanation processes. Catal. Today. 356, 471–489. https://doi.org/10.1016/j.cattod.2020.07.023.

Ateka, A., Rodriguez-Vega, P., Erena, J., Aguayo, A.T., Bilbao, J., 2022. A review on the valorization of CO_2. Focusing on the thermodynamics and catalyst design studies of the direct synthesis of dimethyl ether. Fuel Process. Technol. 233, 107310 https://doi.org/10.1016/j.fuproc.2022.107310.

Atsbha, T.A., Yoon, T., Seongho, P., Lee, C., 2021. A review on the catalytic conversion of CO_2 using H_2 for synthesis of CO, methanol, and hydrocarbons. J. CO_2 Util. 44, 101413 https://doi.org/10.1016/j.jcou.2020.101413.

Attada, Y., Velisoju, V.K., Omar, H., Ramirez, A., Casta, P., 2022. Dual experimental and computational approach to elucidate the effect of Ga on Cu/CeO_2–ZrO_2 catalyst for CO_2 hydrogenation. J. CO_2 Util. 65, 102251 https://doi.org/10.1016/j.jcou.2022.102251.

Atzori, L., Cutrufello, M.G., Meloni, D., Monaci, R., Cannas, C., Gazzoli, D., Sini, M.F., Deiana, P., Rombi, E., 2017. CO2 methanation on hard-templated NiO CeO2 mixed oxides. Int. J. Hydrogen Energy. 42, 20689–20702. https://doi.org/10.1016/j.ijhydene.2017.06.198.

Azancot, L., Bobadilla, L.F., Centeno, M.A., Odriozola, A., 2021. IR spectroscopic insights into the coking-resistance effect of potassium on nickel-based catalyst during dry reforming of methane. Appl. Catal. B Environ. 285, 119822 https://doi.org/10.1016/j.apcatb.2020.119822.

Aziz, M.A.A., Jalil, A.A., Triwahyono, S., Ahmad, A., 2015. CO_2 methanation over heterogeneous catalysts: recent progress and future prospects. Green Chem. 17, 2647–2663. https://doi.org/10.1039/C5GC00119F.

Aziz, M.A.A., Jalil, A.A., Triwahyono, S., Sidik, S.M., 2014. Methanation of carbon dioxide on metal-promoted mesostructured silica nanoparticles. Appl. Catal. A Gen. 486, 115–122. https://doi.org/10.1016/j.apcata.2014.08.022.

Azzolina-Jury, F., Bento, D., Henriques, C., Thibault-Starzyk, F., 2017. Chemical engineering aspects of plasma-assisted CO_2 hydrogenation over nickel zeolites under partial vacuum. J. CO_2 Util. 22, 97–109. https://doi.org/10.1016/j.jcou.2017.09.017.

Bacariza, M.C., Bértolo, R., Graça, I., Lopes, J.M., Henriques, C., 2017. The effect of the compensating cation on the catalytic performances of Ni/USY zeolites towards CO_2

methanation. J. CO_2 Util. 21, 280–291. https://doi.org/10.1016/j.jcou.2017.07.020.
Bacariza, M.C., Graça, I., Bebiano, S.S., Lopes, J.M., Henriques, C., 2018. Micro- and mesoporous supports for CO_2 methanation catalysts: a comparison between SBA-15, MCM-41 and USY zeolite. Chem. Eng. Sci. 175, 72–83. https://doi.org/10.1016/j.ces.2017.09.027.
Bacariza, M.C., Graça, I., Lopes, J.M., Henriques, C., 2019. Tuning zeolite properties towards CO_2 methanation: an overview. ChemCatChem 11, 2388–2400. https://doi.org/10.1002/cctc.201900229.
Bahruji, H., Bowker, M., Hutchings, G., Dimitratos, N., Wells, P., Gibson, E., Jones, W., Brookes, C., Morgan, D., Lalev, G., 2016. Pd/ZnO catalysts for direct CO_2 hydrogenation to methanol. J. Catal. 343, 133–146. https://doi.org/10.1016/j.jcat.2016.03.017.
Bahruji, H., Razak, S.A., Mahadi, A.H., Prasetyoko, D., Sholehah, N.A., Jiao, Y., 2022. PdZn on ZSM-5 nanoparticles for CO2 hydrogenation to dimethyl ether: comparative in situ analysis with Pd/TiO2 and PdZn/TiO2. React. Kinet. Mech. Catal. 135, 2973–2991. https://doi.org/10.1007/s11144-022-02307-6.
Bai, S., Shao, Q., Wang, P., Dai, Q., Wang, X., Huang, X., 2017. Highly active and selective hydrogenation of CO_2 to ethanol by ordered Pd-Cu nanoparticles. J. Am. Chem. Soc. 139, 6827–6830. https://doi.org/10.1021/jacs.7b03101.
Barrios, A.J., Peron, D.V., Chakkingal, A., Dugulan, A.I., Moldovan, S., Nakouri, K., Thuriot-roukos, J., Wojcieszak, R., Thybaut, J.W., Virginie, M., Khodakov, A.Y., 2022. Efficient promoters and reaction paths in the CO_2 Hydrogenation to light olefins over zirconia-supported iron catalysts. ACS Catal 12, 3211–3225. https://doi.org/10.1021/acscatal.1c05648.
Bian, Z., Chan, Y.M., Yu, Y., Kawi, S., 2018. Morphology dependence of catalytic properties of Ni/CeO_2 for CO_2 methanation: a kinetic and mechanism study. Catal. Today. 347, 31–38. https://doi.org/10.1016/j.cattod.2018.04.067.
Burger, T., Koschany, F., Thomys, O., Köhler, K., Hinrichsen, O., 2018. CO_2 methanation over Fe- and Mn-promoted co-precipitated Ni-Al catalysts : synthesis, characterization and catalysis study. Appl. Catal. A, Gen. 558, 44–54. https://doi.org/10.1016/j.apcata.2018.03.021.
Cai, M., Wen, J., Chu, W., Cheng, X., Li, Z., 2011. Methanation of carbon dioxide on Ni/ZrO_2-Al_2O_3 catalysts: effects of ZrO_2 promoter and preparation method of novel ZrO_2-Al_2O_3 carrier. J. Nat. Gas Chem. 20, 318–324. https://doi.org/10.1016/S1003-9953(10)60187-9.
Caparrós, F.J., Soler, L., Rossell, M.D., Angurell, I., Piccolo, L., Rossell, O., Llorca, J., 2018. Remarkable carbon dioxide hydrogenation to ethanol on a palladium/iron oxide single-atom catalyst. ChemCatChem 10, 2365–2369. https://doi.org/10.1002/cctc.201800362.
Chaipraditgul, N., Numpilai, T., Kui Cheng, C., Siri-Nguan, N., Sornchamni, T., Wattanakit, C., Limtrakul, J., Witoon, T., 2021. Tuning interaction of surface-adsorbed species over Fe/K-Al_2O_3 modified with transition metals (Cu, Mn, V, Zn or Co) on light olefins production from CO2 hydrogenation. Fuel 283, 119248. https://doi.org/10.1016/j.fuel.2020.119248.
Chong, C.C., Cheng, Y.W., Setiabudi, H.D., Ainirazali, N., Vo, D.N., Abdullah, B., 2020. Dry reforming of methane over Ni/dendritic fibrous SBA-15 (Ni/DFSBA-15): optimization, mechanism, and regeneration studies. Int. J. Hydrogen Energy. 45, 8507–8525. https://doi.org/10.1016/j.ijhydene.2020.01.056.
Cuellar-Franca, R.M., Azapagic, A., 2015. Carbon capture, storage and utilisation technologies: a critical analysis and comparison of their life cycle environmental impacts. J. CO_2 Util. 9, 82–102. https://doi.org/10.1016/j.jcou.2014.12.001.
Daroughegi, R., Meshkani, F., Rezaei, M., 2021. Enhanced low-temperature activity of CO_2 methanation over ceria-promoted Ni-Al_2O_3 nanocatalyst. Chem. Eng. Sci. 230, 116194 https://doi.org/10.1016/j.ces.2020.116194.
Debek, R., Radlik, M., Motak, M., Elena, M., Turek, W., Da, P., Grzybek, T., 2015. Ni-containing Ce-promoted hydrotalcite derived materials as catalysts for methane reforming with carbon dioxide at low temperature – On the effect of basicity. Catal. Today. 59–66. https://doi.org/10.1016/j.cattod.2015.03.017.
Dejhosseini, M., Aida, T., Watanabe, M., Takami, S., Hojo, D., Aoki, N., Arita, T., Kishita, A., Adschiri, T., 2013. Catalytic cracking reaction of heavy oil in the presence of cerium oxide nanoparticles in supercritical water. Energy and Fuels 27, 4624–4631. https://doi.org/10.1021/ef400855k.
Delmelle, R., Duarte, R.B., Franken, T., Burnat, D., Holzer, L., Borgschulte, A., Heel, A., 2016. Development of improved nickel catalysts for sorption enhanced CO_2 methanation. Int. J. Hydrogen Energy. 41, 20185–20191. https://doi.org/10.1016/j.ijhydene.2016.09.045.
Ding, J., Huang, L., Gong, W., Fan, M., Zhong, Q., Russell, A.G., Gu, H., Zhang, H., Zhang, Y., ping Ye, R., 2019. CO2 hydrogenation to light olefins with high-performance Fe0.30Co0.15Zr0.45K0.10O1.63. J. Catal. 377, 224–232. https://doi.org/10.1016/j.jcat.2019.07.036.
Ding, J., Zhao, W., Zi, L., Xu, X., Liu, Q., Zhong, Q., Xu, Y., 2020a. Promotional effect of ZrO_2 on supported FeCoK catalysts for ethylene synthesis from catalytic CO_2 hydrogenation. Int. J. Hydrogen Energy. 45, 15254–15262. https://doi.org/10.1016/j.ijhydene.2020.03.249.
Ding, L., Shi, T., Gu, J., Cui, Y., Zhang, Z., Yang, C., Chen, T., Lin, M., Wang, P., Xue, N., Peng, L., Guo, X., Zhu, Y., Chen, Z., Ding, W., 2020b. CO2 Hydrogenation to Ethanol over Cu@Na-Beta. Chem 6, 2673–2689. https://doi.org/10.1016/j.chempr.2020.07.001.
Dorner, R.W., Hardy, D.R., Williams, F.W., Davis, B.H., Willauer, H.D., 2009. Influence of gas feed composition and pressure on the catalytic conversion of CO_2 to hydrocarbons using a traditional cobalt-Based fischer-Tropsch catalyst. Energy and Fuels 23, 4190–4195. https://doi.org/10.1021/ef900275m.
Elishav, O., Shener, Y., Beilin, V., Landau, M.V., Herskowitz, M., Shter, G.E., Grader, G. S., Grader, G.S., 2020. Electrospun Fe-Al-O Nanobelts for Selective CO_2 Hydrogenation to Light Olefins. ACS Appl. Mater. Interfaces. 12, 24855–24867. https://doi.org/10.1021/acsami.0c05765.
Erdőhelyi, A., 2020. Hydrogenation of carbon dioxide on supported RH catalysts. Catalysts 10, 1–24. https://doi.org/10.3390/catal10020155.
Fan, W.K., Tahir, M., 2021. Recent trends in developments of active metals and heterogenous materials for catalytic CO_2 hydrogenation to renewable methane: a review. J. Environ. Chem. Eng. 9, 105460 https://doi.org/10.1016/j.jece.2021.105460.
Fan, W.K., Tahir, M., 2022. Recent developments in photothermal reactors with understanding on the role of light/heat for CO_2 hydrogenation to fuels: a review. Chem. Eng. J. 427, 131617 https://doi.org/10.1016/j.cej.2021.131617.
Ferreira-Aparicio, P., Rodriguez-Ramos, I., Anderson, J.A., Guerrero-Ruiz, A., 2000. Mechanistic aspects of the dry reforming of methane over ruthenium catalysts. Appl. Catal. A Gen. 202, 183–196.
Frontera, P., Macario, A., Monforte, G., Bonura, G., Ferraro, M., Dispenza, G., Antonucci, V., Aricò, A.S., Antonucci, P.L., 2017. The role of Gadolinia doped ceria support on the promotion of CO_2 methanation over Ni and Ni–Fe catalysts. Int. J. Hydrogen Energy. 42, 26828–26842. https://doi.org/10.1016/j.ijhydene.2017.09.025.
Frusteri, F., Frusteri, L., Costa, F., Mezzapica, A., Cannilla, C., Bonura, G., 2017. Methane production by sequential supercritical gasification of aqueous organic compounds and selective CO_2 methanation. Appl. Catal. A Gen. 545, 24–32. https://doi.org/10.1016/j.apcata.2017.07.030.
Fu, L., Ren, Z., Si, W., Ma, Q., Huang, W., Liao, K., Huang, Z., Wang, Y., Li, J., Xu, P., 2022. Research progress on CO_2 capture and utilization technology. J. CO_2 Util. 66, 102260 https://doi.org/10.1016/j.jcou.2022.102260.
Fukuhara, C., Hayakawa, K., Suzuki, Y., Kawasaki, W., Watanabe, R., 2017. A novel nickel-based structured catalyst for CO_2 methanation: a honeycomb-type Ni/CeO_2 catalyst to transform greenhouse gas into useful resources. Appl. Catal. A Gen. 532, 12–18. https://doi.org/10.1016/j.apcata.2016.11.036.
Gac, W., Zawadzki, W., Rotko, M., Słowik, G., Greluk, M., 2019. CO2 methanation in the presence of Ce-promoted alumina supported nickel catalysts: H2S deactivation studies. Top. Catal. 62, 524–534. https://doi.org/10.1007/s11244-019-01148-3.
Geng, F., Bonita, Y., Jain, V., Magiera, M., Rai, N., Hicks, J.C., 2020. Bimetallic Ru-Mo phosphide catalysts for the hydrogenation of CO_2 to methanol. Ind. Eng. Chem. Res. 59, 6931–6943. https://doi.org/10.1021/acs.iecr.9b06937.
Gogate, M.R., Davis, R.J., 2010. Comparative study of CO and CO_2 hydrogenation over supported Rh-Fe catalysts. Catal. Commun. 11, 901–906. https://doi.org/10.1016/j.catcom.2010.03.020.
Graça, I., González, L.V., Bacariza, M.C., Fernandes, A., Henriques, C., Lopes, J.M., Ribeiro, M.F., 2014. CO2 hydrogenation into CH4 on NiHNaUSY zeolites. Appl. Catal. B Environ 147, 101–110. https://doi.org/10.1016/j.apcatb.2013.08.010.
Gu, H., Ding, J., Zhong, Q., Zeng, Y., Song, F., 2019. Promotion of surface oxygen vacancies on the light olefins synthesis from catalytic CO_2 hydrogenation over Fe-K/ZrO_2 catalysts. Int. J. Hydrogen Energy. 44, 11808–11816. https://doi.org/10.1016/j.ijhydene.2019.03.046.
Guilera, J., Valle, J., Alarcón, A., Díaz, J.A., Andreu, T., 2019. Metal-oxide promoted Ni/Al2O3 as CO_2 methanation micro-size catalysts. J. CO_2 Util 30, 11–17. https://doi.org/10.1016/j.jcou.2019.01.003.
Gutterød, E.S., Lazzarini, A., Fjermestad, T., Kaur, G., Manzoli, M., Bordiga, S., Svelle, S., Lillerud, K.P., Skúlason, E., Øien-ØDegaard, S., Nova, A., Olsbye, U., 2020. Hydrogenation of CO_2 to methanol by Pt nanoparticles encapsulated in UiO-67: deciphering the role of the metal-organic framework. J. Am. Chem. Soc. 142, 999–1009. https://doi.org/10.1021/jacs.9b10873.
Hamid, M.Y.S., Firmansyah, M.L., Triwahyono, S., Jalil, A.A., Mukti, R.R., Febriyanti, E., Suendo, V., Setiabudi, H.D., Mohamed, M., Nabgan, W., 2017. Oxygen vacancy-rich mesoporous silica KCC-1 for CO_2 methanation. Appl. Catal. A Gen. 532, 86–94. https://doi.org/10.1016/j.apcata.2016.12.023.
Han, Y., Fang, C., Ji, X., Wei, J., Ge, Q., Sun, J., 2020. Interfacing with carbonaceous potassium promoters boosts catalytic CO_2 hydrogenation of iron. ACS Catal 10, 12098–12108. https://doi.org/10.1021/acscatal.0c03215.
He, Z., Qian, Q., Ma, J., Meng, Q., Zhou, H., Song, J., Liu, Z., Han, B., 2016. Water-enhanced synthesis of higher alcohols from CO_2 hydrogenation over a Pt/Co_3O_4 catalyst under milder conditions. Angew. Chemie. 128, 747–751. https://doi.org/10.1002/ange.201507585.
Hossen, M.A., Solayman, H.M., Leong, K.H., Sim, L.C., Yaacof, N., Aziz, A.A., Wu, L., Monir, M.U., 2022. Recent progress in TiO_2-Based photocatalysts for conversion of CO_2 to hydrocarbon fuels: a systematic review. Results Eng. 16, 100795 https://doi.org/10.1016/j.rineng.2022.100795.
Hu, X., Lu, G., 2009. Inhibition of methane formation in steam reforming reactions through modification of Ni catalyst and the reactants. Green Chem. 11, 724–773. https://doi.org/10.1039/b814009j.
Huang, Y., Meng, X., Dang, Z., Weng, S., Zhang, C., 1995. Light olefin synthesis from carbon dioxide by hydrogenation over $Fe_3(CO)_{12}$ supported on ZSM-5 zeolite catalyst. J. Chem. Soc. Chem. Commun. 3, 1025–1026. https://doi.org/10.1039/C39950001025.
I.E. Agency, World Energy Outlook, 2022.
Inui, T., Yamamoto, T., Inoue, M., Hara, H., Takeguchi, T., Kim, J.B., 1999. Highly effective synthesis of ethanol by CO_2-hydrogenation on well balanced multi-functional FT-type composite catalysts. Appl. Catal. A Gen. 186, 395–406. https://doi.org/10.1016/S0926-860X(99)00157-X.
Jalama, K., 2017. Carbon dioxide hydrogenation over nickel-, ruthenium-, and copper-based catalysts: review of kinetics and mechanism. Catal. Rev. - Sci. Eng. 59, 95–164. https://doi.org/10.1080/01614940.2017.1316172.

Janke, C., Duyar, M.S., Hoskins, M., Farrauto, R., 2014. Catalytic and adsorption studies for the hydrogenation of CO_2 to methane. Appl. Catal. B Environ. 152–153, 184–191. https://doi.org/10.1016/j.apcatb.2014.01.016.

Jia, X., Zhang, X., Rui, N., Hu, X., jun Liu, C., 2019. Structural effect of Ni/ZrO_2 catalyst on CO_2 methanation with enhanced activity. Appl. Catal. B Environ. 244, 159–169. https://doi.org/10.1016/j.apcatb.2018.11.024.

Jiang, J., Wen, C., Tian, Z., Wang, Y., Zhai, Y., Chen, L., Li, Y., Liu, Q., Wang, C., Ma, L., 2020. Manganese-promoted Fe_3O_4 microsphere for efficient conversion of CO_2 to light olefins. Ind. Eng. Chem. Res. 59, 2155–2162. https://doi.org/10.1021/acs.iecr.9b05342.

Jomjaree, T., Sintuya, P., Srifa, A., Koo-amornpattana, W., Kiatphuengporn, S., Assabumrungrat, S., Sudoh, M., Watanabe, R., Fukuhara, C., Ratchahat, S., 2020. Catalytic performance of Ni catalysts supported on CeO_2 with different morphologies for low-temperature CO_2 methanation. Catal. Today. https://doi.org/10.1016/j.cattod.2020.08.010.

Kangvansura, P., Chew, L.M., Kongmark, C., Santawaja, P., Ruland, H., Xia, W., Schulz, H., Worayingyong, A., Muhler, M., 2017. Effects of potassium and manganese promoters on nitrogen-doped carbon nanotube-supported iron catalysts for CO_2 hydrogenation. Engineering 3, 385–392. https://doi.org/10.1016/J.ENG.2017.03.013.

Keen, W., Tahir, M., 2022. Recent advances on cobalt metal organic frameworks (MOFs) for photocatalytic CO_2 reduction to renewable energy and fuels: a review on current progress and future directions. Energy Convers. Manag. 253, 115180 https://doi.org/10.1016/j.enconman.2021.115180.

Kim, K.Y., Lee, H., Noh, W.Y., Shin, J., Han, S.J., Kim, S.K., An, K., Lee, J.S., 2020. Cobalt ferrite nanoparticles to form a catalytic Co-Fe alloy carbide phase for selective CO_2 hydrogenation to light olefins. ACS Catal. 10, 8660–8671. https://doi.org/10.1021/acscatal.0c01417.

Kusama, H., Okabe, K., Sayama, K., Arakawa, H., 1996. CO2 hydrogenation to ethanol over promoted Rh/SiO2 catalysts. Catal. Today. 28, 261–266. https://doi.org/10.1016/0920-5861(95)00246-4.

Kusama, H., Okabe, K., Sayama, K., Arakawa, H., 1997. Ethanol synthesis by catalytic hydrogenation of CO_2 over Rh-Fe/SiO_2 catalysts. Energy 22, 343–348. https://doi.org/10.1016/S0360-5442(96)00095-3.

Lda, F., The, V., Lda, F., Carlo, M., 1999. A direct-methane fuel cell with a ceria-based anode. Nature 400, 649–651.

Le, M.C., Van, K.Le, Nguyen, T.H.T., Nguyen, N.H., 2017a. The impact of Ce-Zr addition on nickel dispersion and catalytic behavior for CO_2 methanation of Ni/AC catalyst at low temperature. J. Chem. 2017. https://doi.org/10.1155/2017/4361056.

Le, T.A., Kim, M.S., Lee, S.H., Kim, T.W., Park, E.D., 2017b. CO and CO_2 methanation over supported Ni catalysts. Catal. Today. 293–294, 89–96. https://doi.org/10.1016/j.cattod.2016.12.036.

Le, T.A., Kim, T.W., Lee, S.H., Park, E.D., 2018. Effects of Na content in Na/Ni/SiO_2 and Na/Ni/CeO_2 catalysts for CO and CO_2 methanation. Catal. Today. 303, 159–167. https://doi.org/10.1016/j.cattod.2017.09.031.

Lechkar, A., Barroso Bogeat, A., Blanco, G., Pintado, J.M., Soussi el Begrani, M., 2018. Methanation of carbon dioxide over ceria-praseodymia promoted Ni-alumina catalysts. Influence of metal loading, promoter composition and alumina modifier. Fuel 234, 1401–1413. https://doi.org/10.1016/j.fuel.2018.07.157.

Li, M., Amari, H., van Veen, A.C., 2018. Metal-oxide interaction enhanced CO_2 activation in methanation over ceria supported nickel nanocrystallites. Appl. Catal. B Environ. 239, 27–35. https://doi.org/10.1016/j.apcatb.2018.07.074.

Li, X., Wu, M., Lai, Z., He, F., 2005. Studies on nickel-based catalysts for carbon dioxide reforming of methane. Appl. Catal. A Gen. 290, 81–86. https://doi.org/10.1016/j.apcata.2005.05.021.

Liang, B., Duan, H., Sun, T., Ma, J., Liu, X., Xu, J., Su, X., Huang, Y., Zhang, T., 2019a. Effect of Na promoter on Fe-based catalyst for CO_2 hydrogenation to Alkenes. ACS Sustain. Chem. Eng. 7, 925–932. https://doi.org/10.1021/acssuschemeng.8b04538.

Liang, B., Sun, T., Ma, J., Duan, H., Li, L., Yang, X., Zhang, Y., Su, X., Huang, Y., Zhang, T., 2019b. Mn decorated Na/Fe catalysts for CO_2 hydrogenation to light olefins. Catal. Sci. Technol. 9, 456–464. https://doi.org/10.1039/c8cy02275e.

Liu, B., Geng, S., Zheng, J., Jia, X., Jiang, F., Liu, X., 2018. Unravelling the new roles of Na and Mn promoter in CO_2 hydrogenation over Fe_3O_4-based catalysts for enhanced selectivity to light α-Olefins. ChemCatChem 10, 4718–4732. https://doi.org/10.1002/cctc.201800782.

Liu, H., Zou, X., Wang, X., Lu, X., Ding, W., 2012. Effect of CeO_2 addition on Ni/Al_2O_3 catalysts for methanation of carbon dioxide with hydrogen. J. Nat. Gas Chem. 21, 703–707. https://doi.org/10.1016/S1003-9953(11)60422-2.

Liu, Q., Tian, Y., 2017. One-pot synthesis of NiO/SBA-15 monolith catalyst with a three-dimensional framework for CO_2 methanation. Int. J. Hydrogen Energy. 42, 12295–12300. https://doi.org/10.1016/j.ijhydene.2017.02.070.

Liu, S., He, Y., Fu, W., Chen, J., Ren, J., Liao, L., Sun, R., Tang, Z., Mebrahtu, C., Zeng, F., 2023. Hetero-site cobalt catalysts for higher alcohols synthesis by CO_2 hydrogenation: a review. J. CO_2 Util. 67, 102322 https://doi.org/10.1016/j.jcou.2022.102322.

Liu, Z., Gao, X., Liu, B., Ma, Q., Zhao, T., Zhang, J., 2022. Recent advances in thermal catalytic CO_2 methanation on hydrotalcite-derived catalysts. Fuel 321, 124115. https://doi.org/10.1016/j.fuel.2022.124115.

Lu, H., Yang, X., Gao, G., Wang, J., Han, C., Liang, X., Li, C., Li, Y., Zhang, W., Chen, X., 2016. Metal (Fe, Co, Ce or La) doped nickel catalyst supported on ZrO_2 modified mesoporous clays for CO and CO_2 methanation. Fuel 183, 335–344. https://doi.org/10.1016/j.fuel.2016.06.084.

Majhi, S.M., Lee, H.J., Choi, H.N., Cho, H.Y., Kim, J.S., Lee, C.R., Yu, Y.T., 2019. Construction of novel hybrid PdO-ZnO p-n heterojunction nanostructures as a high-response sensor for acetaldehyde gas. CrystEngComm 21, 5084–5094. https://doi.org/10.1039/c9ce00710e.

Makdee, A., Chanapattharapol, K.C., Kidkhunthod, P., Poo-Arporn, Y., Ohno, T., 2020. The role of Ce addition in catalytic activity enhancement of TiO_2-supported Ni for CO_2 methanation reaction. RSC Adv. 10, 26952–26971. https://doi.org/10.1039/d0ra04934d.

Martínez, J., Hernández, E., Alfaro, S., Medina, R.L., Aguilar, G.V., Albiter, E., Valenzuela, M.A., 2019. High Selectivity and Stability of Nickel Catalysts For CO_2 Methanation: Support effects. Catalysts, p. 9. https://doi.org/10.3390/catal9010024.

Mebrahtu, C., Abate, S., Perathoner, S., Chen, S., Centi, G., 2018. CO2 methanation over Ni catalysts based on ternary and quaternary mixed oxide: a comparison and analysis of the structure-activity relationships. Catal. Today. 304, 181–189. https://doi.org/10.1016/j.cattod.2017.08.060.

Miao, B., Ma, S.S.K., Wang, X., Su, H., Chan, S.H., 2016. Catalysis mechanisms of CO_2 and CO methanation. Catal. Sci. Technol. 6, 4048–4058. https://doi.org/10.1039/c6cy00478d.

Mutschler, R., Moioli, E., Luo, W., Gallandat, N., Züttel, A., 2018. CO2 hydrogenation reaction over pristine Fe, Co, Ni, Cu and Al2O3 supported Ru: comparison and determination of the activation energies. J. Catal. 366, 139–149. https://doi.org/10.1016/j.jcat.2018.08.002.

Nakamura, J., Aikawa, K., Sato, K., Uchijima, T., 1994. Role of support in reforming of CH_4 with CO2 over Rh catalysts. Catal. Lett. 25, 265–270.

Nezam, I., Zhou, W., Gusmao, G.S., Realff, M.J., Wang, Y., Medford, A.J., Jones, C.W., 2021. Direct aromatization of CO_2 via combined CO_2 hydrogenation and zeolite-based acid catalysis. J. CO_2 Util. 45, 101405 https://doi.org/10.1016/j.jcou.2020.101405.

Niu, J., Liu, H., Jin, Y., Fan, B., Qi, W., 2022. Comprehensive review of Cu-based CO_2 hydrogenation to CH_3OH: insights from experimental work and theoretical analysis. Int. J. Hydrogen Energy. 47, 9183–9200. https://doi.org/10.1016/j.ijhydene.2022.01.021.

Nizio, M., Benrabbah, R., Krzak, M., Debek, R., Motak, M., Cavadias, S., Gálvez, M.E., Costa, P.Da, 2016. Low temperature hybrid plasma-catalytic methanation over Ni-Ce-Zr hydrotalcite-derived catalysts. Catal. Commun. 83, 14–17. https://doi.org/10.1016/j.catcom.2016.04.023.

Numpilai, T., Witoon, T., Chanlek, N., Limphirat, W., Bonura, G., Chareonpanich, M., Limtrakul, J., 2017. Structure–activity relationships of Fe-Co/K-Al_2O_3 catalysts calcined at different temperatures for CO_2 hydrogenation to light olefins. Appl. Catal. A Gen. 547, 219–229. https://doi.org/10.1016/j.apcata.2017.09.006.

Ojelade, O.A., Zaman, S.F., 2021. A review on CO_2 hydrogenation to lower olefins: understanding the structure-property relationships in heterogeneous catalytic systems. J. CO_2 Util. 47, 101506 https://doi.org/10.1016/j.jcou.2021.101506.

Panagiotopoulou, P., 2017. Hydrogenation of CO_2 over supported noble metal catalysts. Appl. Catal. A Gen. 542, 63–70. https://doi.org/10.1016/j.apcata.2017.05.026.

Pastor-Pérez, L., Saché, E.Le, Jones, C., Gu, S., Arellano-Garcia, H., Reina, T.R., 2018. Synthetic natural gas production from CO_2 over Ni-x/CeO_2-ZrO_2 (x = Fe, Co) catalysts: influence of promoters and space velocity. Catal. Today. 317, 108–113. https://doi.org/10.1016/j.cattod.2017.11.035.

Perkas, N., Amirian, G., Zhong, Z., Teo, J., Gofer, Y., Gedanken, A., 2009. Methanation of carbon dioxide on ni catalysts on mesoporous ZrO_2 doped with rare earth oxides. Catal. Lett. 130, 455–462. https://doi.org/10.1007/s10562-009-9952-8.

Petala, A., Panagiotopoulou, P., 2018. Methanation of CO_2 over alkali-promoted Ru/TiO_2 catalysts: I. Effect of alkali additives on catalytic activity and selectivity. Appl. Catal. B Environ. 224, 919–927. https://doi.org/10.1016/j.apcatb.2017.11.048.

Quindimil, A., De-La-Torre, U., Pereda-Ayo, B., Davó-Quiñonero, A., Bailón-García, E., Lozano-Castelló, D., González-Marcos, J.A., Bueno-López, A., González-Velasco, J.R., 2020. Effect of metal loading on the CO_2 methanation: a comparison between alumina supported Ni and Ru catalysts. Catal. Today. 356, 419–432. https://doi.org/10.1016/j.cattod.2019.06.027.

Quindimil, A., De-La-Torre, U., Pereda-Ayo, B., González-Marcos, J.A., González-Velasco, J.R., 2018. Ni catalysts with La as promoter supported over Y- and BETA-zeolites for CO_2 methanation. Appl. Catal. B Environ. 238, 393–403. https://doi.org/10.1016/j.apcatb.2018.07.034.

Raza, S., Orooji, Y., Ghasali, E., Hayat, A., Karimi-maleh, H., Lin, H., 2023. Engineering approaches for CO_2 converting to biomass coupled with nanobiomaterials as biomediated towards circular bioeconomy. J. CO_2 Util. 67, 102295 https://doi.org/10.1016/j.jcou.2022.102295.

Ren, J., Mebrahtu, C., Palkovits, R., 2020. Ni-based catalysts supported on Mg-Al hydrotalcites with different morphologies for CO_2 methanation: exploring the effect of metal-support interaction. Catal. Sci. Technol. 10, 1902–1913. https://doi.org/10.1039/c9cy02523e.

Ritchie, H., Roser, M., Rosado, P., 2020. CO_2 and Greenhouse Gas Emissions. Our World Data. Accessed: Dec. 19, 2022. [Online]. Available. https://ourworldindata.org/emissions-by-sector.

Ruiz-Lopez, E., Gandara-Loe, J., Baena-Moreno, F., Reina, T.R., Odriozola, J.A., 2022. Electrocatalytic CO_2 conversion to C_2 products: catalysts design, market perspectives and techno-economic aspects. Renew. Sustain. Energy Rev. 161, 112329 https://doi.org/10.1016/j.rser.2022.112329.

Sakpal, T., Lefferts, L., 2018. Structure-dependent activity of CeO_2 supported Ru catalysts for CO_2 methanation. J. Catal. 367, 171–180. https://doi.org/10.1016/j.jcat.2018.08.027.

Satthawong, R., Koizumi, N., Song, C., Prasassarakich, P., 2013. Bimetallic Fe-Co catalysts for CO_2 hydrogenation to higher hydrocarbons. J. CO_2 Util 3–4, 102–106. https://doi.org/10.1016/j.jcou.2013.10.002.

Satthawong, R., Koizumi, N., Song, C., Prasassarakich, P., 2015. Light olefin synthesis from CO_2 hydrogenation over K-promoted Fe-Co bimetallic catalysts. Catal. Today. 251, 34–40. https://doi.org/10.1016/j.cattod.2015.01.011.

Schaaf, T., Grünig, J., Schuster, M.R., Rothenfluh, T., Orth, A., 2014. Methanation of CO_2- storage of renewable energy in a gas distribution system. Energy. Sustain. Soc. 4, 1–14. https://doi.org/10.1186/s13705-014-0029-1.

Sedighi, M., Mohammadi, M., 2020. CO2 hydrogenation to light olefins over Cu-CeO2/SAPO-34 catalysts: product distribution and optimization. J. CO_2 Util. 35, 236–244. https://doi.org/10.1016/j.jcou.2019.10.002.

Shao, S., Cui, C., Tang, Z., Li, G., 2022. Recent advances in metal-organic frameworks for catalytic CO_2 hydrogenation to diverse products. Nano Res. 15, 10110–10133.

Sharma, D., Sharma, R., Chand, D., Chaudhary, A., 2022. Nanocatalysts as potential candidates in transforming CO_2 into valuable fuels and chemicals: a review. Environ. Nanotechnology, Monit. Manag. 18, 100671 https://doi.org/10.1016/j.enmm.2022.100671.

Sholeha, N.A., Jannah, L., Rohma, H.N., Widiastuti, N., Prasetyoko, D., Jalil, A.A., Bahruji, H., 2020. Synthesis of zeolite NaY from dealuminated metakaolin as Ni support for CO_2 hydrogenation to methane. Clays Clay Miner 68, 513–523. https://doi.org/10.1007/s42860-020-00089-3.

Sholeha, N.A., Mohamad, S., Bahruji, H., Prasetyoko, D., Widiastuti, N., Abdul Fatah, N. A., Jalil, A.A., Taufiq-Yap, Y.H., 2021. Enhanced CO_2 methanation at mild temperature on Ni/zeolite from kaolin: effect of metal-support interface. RSC Adv. 11, 16376–16387. https://doi.org/10.1039/d1ra01014j.

Solymosi, F., Erdöhelyi, A., Bánsági, T., 1981. Infrared study of the surface interaction between H_2 and CO_2 over rhodium on various supports. J. Chem. Soc. Faraday Trans. 1 Phys. Chem. Condens. Phases. 77, 2645–2657. https://doi.org/10.1039/F19817702645.

Sun, Y., Zhang, G., Liu, J., Xu, Y., Lv, Y., 2020. Production of syngas via CO_2 methane reforming process: effect of cerium and calcium promoters on the performance of Ni-MSC catalysts. Int. J. Hydrogen Energy. 45, 640–649. https://doi.org/10.1016/j.ijhydene.2019.10.228.

Tada, S., Ikeda, S., Shimoda, N., Honma, T., Takahashi, M., Nariyuki, A., Satokawa, S., 2017. Sponge Ni catalyst with high activity in CO_2 methanation. Int. J. Hydrogen Energy. 42, 30126–30134. https://doi.org/10.1016/j.ijhydene.2017.10.138.

Takano, H., Izumiya, K., Kumagai, N., Hashimoto, K., 2011. The effect of heat treatment on the performance of the Ni/(Zr-Sm oxide) catalysts for carbon dioxide methanation. Appl. Surf. Sci. 257, 8171–8176. https://doi.org/10.1016/j.apsusc.2011.01.141.

Takano, H., Kirihata, Y., Izumiya, K., Kumagai, N., Habazaki, H., Hashimoto, K., 2016. Highly active Ni/Y-doped ZrO_2 catalysts for CO_2 methanation. Appl. Surf. Sci. 388, 653–663. https://doi.org/10.1016/j.apsusc.2015.11.187.

Takano, H., Shinomiya, H., Izumiya, K., Kumagai, N., 2015. CO2 methanation of Ni catalysts supported on tetragonal ZrO2 doped with Ca2+ and Ni2+ ions. Int. J. Hydrogen Energy. 40, 8347–8355. https://doi.org/10.1016/j.ijhydene.2015.04.128.

Teh, L.P., Triwahyono, S., Jalil, A.A., Mukti, R.R., Aziz, M.A.A., Shishido, T., 2015. Mesoporous ZSM-5 having both intrinsic acidic and basic sites for cracking and methanation. Chem. Eng. J. 270, 196–204. https://doi.org/10.1016/j.cej.2015.01.084.

Tountas, A.A., Peng, X., Tavasoli, A.V., Duchesne, P.N., Dingle, T.L., Dong, Y., Hurtado, L., Mohan, A., Sun, W., Ulmer, U., Wang, L., Wood, T.E., Maravelias, C.T., Sain, M.M., Ozin, G.A., 2019. Towards solar methanol: past, present, and future. Adv. Sci 6, 1801903. https://doi.org/10.1002/advs.201801903.

Valinejad Moghaddam, S., Rezaei, M., Meshkani, F., Daroughegi, R., 2018. Carbon dioxide methanation over Ni-M/Al_2O_3 (M: fe, CO, Zr, La and Cu) catalysts synthesized using the one-pot sol-gel synthesis method. Int. J. Hydrogen Energy 43, 16522–16533. https://doi.org/10.1016/j.ijhydene.2018.07.013.

Vecchietti, J., Bonivardi, A., Xu, W., Stacchiola, D.J., Delgado, J.J., Calatayud, M., Collins, S.E., 2014. Understanding the role of oxygen vacancies in the water gas shift reaction on ceria-supported platinum catalysts. ACS Catal. https://doi.org/10.1021/cs500323u.

Vita, A., Italiano, C., Pino, L., Frontera, P., Ferraro, M., Antonucci, V., 2018. Activity and stability of powder and monolith-coated Ni/GDC catalysts for CO_2 methanation. Appl. Catal. B Environ. 226, 384–395. https://doi.org/10.1016/j.apcatb.2017.12.078.

Vourros, A., Garagounis, I., Kyriakou, V., Carabineiro, S.A.C., Maldonado-Hódar, F.J., Marnellos, G.E., Konsolakis, M., 2017. Carbon dioxide hydrogenation over supported Au nanoparticles: effect of the support. J. CO_2 Util 19, 247–256. https://doi.org/10.1016/j.jcou.2017.04.005.

Vrijburg, W.L., Garbarino, G., Chen, W., Parastaev, A., Longo, A., Pidko, E.A., Hensen, E. J.M., 2020. Ni-Mn catalysts on silica-modified alumina for CO_2 methanation. J. Catal. 382, 358–371. https://doi.org/10.1016/j.jcat.2019.12.026.

Wang, D., Bi, Q., Yin, G., Zhao, W., Huang, F., Xie, X., Jiang, M., 2016a. Direct synthesis of ethanol via CO_2 hydrogenation using supported gold catalysts. Chem. Commun. 52, 14226–14229. https://doi.org/10.1039/c6cc08161d.

Wang, F., He, S., Chen, H., Wang, B., Zheng, L., Wei, M., Evans, D.G., Duan, X., 2016b. Active Site Dependent Reaction Mechanism over Ru/CeO_2 Catalyst toward CO_2 Methanation. J. Am. Chem. Soc. 138, 6298–6305. https://doi.org/10.1021/jacs.6b02762.

Wang, L., He, S., Wang, L., Lei, Y., Meng, X., Xiao, F.S., 2019. Cobalt-nickel catalysts for selective hydrogenation of carbon dioxide into ethanol. ACS Catal 9, 11335–11340. https://doi.org/10.1021/acscatal.9b04187.

Wang, L., Wang, L., Zhang, J., Liu, X., Wang, H., Zhang, W., Yang, Q., Ma, J., Dong, X., Yoo, S.J., Kim, J.G., Meng, X., Xiao, F.S., 2018a. Selective hydrogenation of CO_2 to ethanol over cobalt catalysts. Angew. Chemie - Int. Ed. 57, 6104–6108. https://doi.org/10.1002/anie.201800729.

Wang, W., Jiang, X., Wang, X., Song, C., 2018b. Fe-Cu bimetallic catalysts for selective CO_2 hydrogenation to Olefin-Rich C_{2+} hydrocarbons. Ind. Eng. Chem. Res. 57, 4535–4542. https://doi.org/10.1021/acs.iecr.8b00016.

Wang, X., Chen, Q., Zhou, Y., Li, H., Fu, J., Liu, M., 2022. Cu-based bimetallic catalysts for CO_2 reduction reaction. Adv. Sens. Energy Mater. 1, 100023 https://doi.org/10.1016/j.asems.2022.100023.

Wei, J., Ge, Q., Yao, R., Wen, Z., Fang, C., Guo, L., Xu, H., Sun, J., 2017. Directly converting CO_2 into a gasoline fuel. Nat. Commun. 8, 15174. https://doi.org/10.1038/ncomms15174.

Wierzbicki, D., Baran, R., Dębek, R., Motak, M., Gálvez, M.E., Grzybek, T., Da Costa, P., Glatzel, P., 2018a. Examination of the influence of La promotion on Ni state in hydrotalcite-derived catalysts under CO_2 methanation reaction conditions: operando X-ray absorption and emission spectroscopy investigation. Appl. Catal. B Environ. 232, 409–419. https://doi.org/10.1016/j.apcatb.2018.03.089.

Wierzbicki, D., Debek, R., Motak, M., Grzybek, T., Gálvez, M.E., Costa, P.Da, 2016. Novel Ni-La-hydrotalcite derived catalysts for CO_2 methanation. Catal. Commun. 83, 5–8. https://doi.org/10.1016/j.catcom.2016.04.021.

Wierzbicki, D., Motak, M., Grzybek, T., Gálvez, M.E., Costa, P.Da, 2018b. The influence of lanthanum incorporation method on the performance of nickel-containing hydrotalcite-derived catalysts in CO_2 methanation reaction. Catal. Today. 307, 205–211. https://doi.org/10.1016/j.cattod.2017.04.020.

Xiao-xing, W., Yong-hong, D., Jun-feng, Z., Yi-sheng, T.A.N., 2022. Catalytic conversion of CO_2 into high value-added hydrocarbons over tandem catalyst. J. Fuel Chem. Technol. 50, 538–563. https://doi.org/10.1016/S1872-5813(21)60181-0.

Xu, D., Ding, M., Hong, X., Liu, G., Tsang, S.C.E., 2020. Selective C_{2+} alcohol synthesis from direct CO_2 hydrogenation over a Cs-promoted Cu-Fe-Zn catalyst. ACS Catal 10, 5250–5260. https://doi.org/10.1021/acscatal.0c01184.

Xu, L., Wang, F., Chen, M., Nie, D., Lian, X., Lu, Z., Chen, H., Zhang, K., Ge, P., 2017. CO2 methanation over rare earth doped Ni based mesoporous catalysts with intensified low-temperature activity. Int. J. Hydrogen Energy. 42, 15523–15539. https://doi.org/10.1016/j.ijhydene.2017.05.027.

Yang, C., Mu, R., Wang, G., Song, J., Tian, H., Zhao, Z.J., Gong, J., 2019. Hydroxyl-mediated ethanol selectivity of CO_2 hydrogenation. Chem. Sci. 10, 3161–3167. https://doi.org/10.1039/c8sc05608k.

Yang, Y., Liu, J., Liu, F., Wu, D., 2020. Reaction mechanism of CO_2 methanation over Rh/TiO_2 catalyst. Fuel 276, 118093. https://doi.org/10.1016/j.fuel.2020.118093.

Ye, R.-P., Ding, J., Gong, W., Argyle, M.D., Zhong, Q., Wang, Y., Russell, C.K., Xu, Z., Russell, A.G., Li, Q., Fan, M., Yao, Y.G., 2019. CO_2 hydrogenation to high-value products via heterogeneous catalysis. Nat. Commun. 5, 5698. https://doi.org/10.1038/s41467-019-13638-9.

Ye, X., Yang, C., Pan, X., Ma, J., Zhang, Y., Ren, Y., Liu, X., Li, L., Huang, Y., 2020. Highly selective hydrogenation of CO_2 to ethanol via designed bifunctional Ir1-In_2O_3 Single-atom catalyst. J. Am. Chem. Soc. 142, 19001–19005. https://doi.org/10.1021/jacs.0c08607.

Yu, F., Deng, K., Du, M., Wang, W., Liu, F., Liang, D., 2023. Electrochemical CO_2 reduction: from catalysts to reactive thermodynamics and kinetics. Carbon Capture Sci. Technol. 6, 100081 https://doi.org/10.1016/j.ccst.2022.100081.

Zhang, F., Li, Y., Qi, M., Yamada, Y.M.A., Anpo, M., Tang, Z., 2021. Photothermal catalytic CO_2 reduction over nanomaterials. Chem. Catal. 1, 272–297. https://doi.org/10.1016/j.checat.2021.01.003.

Zhang, S., Liu, X., Shao, Z., Wang, H., Sun, Y., 2020a. Direct CO_2 hydrogenation to ethanol over supported Co_2C catalysts: studies on support effects and mechanism. J. Catal. 382, 86–96. https://doi.org/10.1016/j.jcat.2019.11.038.

Zhang, Z., Wei, C., Jia, L., Liu, Y., Sun, C., Wang, P., Tu, W., 2020b. Insights into the regulation of FeNa catalysts modified by Mn promoter and their tuning effect on the hydrogenation of CO_2 to light olefins. J. Catal. 390, 12–22. https://doi.org/10.1016/j.jcat.2020.07.020.

Zheng, J.N., An, K., Wang, J.M., Li, J., Liu, Y., 2019. Direct synthesis of ethanol via CO_2 hydrogenation over the Co/La-Ga-O composite oxide catalyst. J. Fuel Chem. Technol. 47, 697–708. https://doi.org/10.1016/s1872-5813(19)30031-3.